scientific reports

Check for updates

OPEN

2-Deoxy-D-Glucose restores glial cell mitochondrial function and attenuates neuroinflammation

Payam Gharibani[1], Yu Guo[2], Shruthi Shanmukha[3], Judy J. Lee[1], Katherine Kopp[4], Paul M. Kim[3] & Michael D. Kornberg[1]✉

Neuroinflammation plays a central role in a wide spectrum of neurological diseases, driven generally by reactive microglia and astrocytes. Inflammatory stimulation of microglia and astrocytes leads to a metabolic shift from oxidative phosphorylation (OXPHOS) to glycolysis, which is required to support pro-inflammatory effector functions. This metabolic reprogramming is associated with impaired mitochondrial dynamics, including reduced biogenesis, increased fragmentation, and loss of membrane potential. Targeting microglia and astrocyte metabolism may offer a novel therapeutic approach for modulating neuroinflammation and restoring homeostatic immune functions. Here, we examined the potential of 2-Deoxy-D-Glucose (2DG), a glycolysis inhibitor, to attenuate neuroinflammation by restoring mitochondrial dynamics. In BV2 and primary glial cultures, low-dose 2DG reversed LPS-induced metabolic reprogramming, restoring OXPHOS, reducing mitochondrial fragmentation, and enhancing biogenesis. In vivo, it preserved spare respiratory capacity and increased complex-V activity in brain mitochondria from LPS-treated mice without affecting oxidative stress. At a mechanistic level, 2DG restored activation of AMP-activated protein kinase, a master regulator of mitochondrial dynamics. In conjunction with these metabolic effects, 2DG suppressed LPS-induced pro-inflammatory gene expression while enhancing markers associated with the resolution of inflammation and tissue repair. Critically, systemic low-dose 2DG reduced neuroinflammation and restored immune homeostasis in two LPS-induced mouse models, highlighting its therapeutic potential in neurological disorders.

Keywords Neuroinflammation, Immunometabolism, 2-Deoxy-D-Glucose, Mitochondrial dynamics, Mitochondrial function

Neuroinflammation is a hallmark of numerous neurological disorders, including Alzheimer's disease, Parkinson's disease, multiple sclerosis[1], and traumatic brain injury[2]. In these conditions, chronic inflammation, primarily driven by activated microglia (MG) and astrocytes, leads to neuroaxonal loss and disease progression[3]. As the primary immune cells in the central nervous system (CNS), MG and astrocytes play key roles in this process by shifting to pro-inflammatory states upon activation, releasing cytokines, chemokines, and other inflammatory mediators[4,5]. Although neuroinflammation acts as a protective response to injury or infection, its prolonged and dysregulated presence drives neural network dysfunction and neurodegenerative processes[6].

Recent studies have emphasized the vital role of metabolic reprogramming in neuroinflammation[1,7–9]. Upon pro-inflammatory activation, glial cells (particularly MG and astrocytes) experience a metabolic shift from oxidative phosphorylation (OXPHOS) to glycolysis to support effector functions and to meet increased energy and biomass demands[7]. While glycolysis is less efficient in ATP production than OXPHOS, it rapidly supplies energy and biosynthetic intermediates needed for immune responses[10]. However, this shift also leads to the accumulation of reactive oxygen species (ROS) and metabolic by-products that drive further inflammation and oxidative stress, creating a vicious cycle that aggravates neuroinflammation and neurodegeneration[10]. A key contributor to this cycle is mitochondrial dysfunction, as dysfunctional mitochondria generate excessive ROS and activate inflammasomes, further propagating the inflammatory response[11]. A promising therapeutic approach for modulating neuroinflammation could therefore be targeting the metabolic pathways involved in glial activation, as this modulation could break the cycle between mitochondrial dysfunction and inflammatory

[1]Department of Neurology, Johns Hopkins University School of Medicine, Baltimore, MD 21287, USA. [2]Department of Biomedical Engineering, Johns Hopkins University School of Medicine, Baltimore, MD 21287, USA. [3]Department of Psychiatry and Behavioral Sciences, Johns Hopkins University School of Medicine, Baltimore, MD 21287, USA. [4]Johns Hopkins University School of Medicine, Baltimore, MD 21287, USA. ✉email: michael.kornberg@jhmi.edu

signaling, shifting glial cells from a pro-inflammatory state to a more anti-inflammatory or regenerative state. Restoring mitochondrial function is particularly imperative, as mitochondria are critical for regulating both energy production and cellular stress responses[11].

In this context, 2-Deoxy-D-glucose (2DG) has emerged as a potential therapeutic agent, known to inhibit glycolysis by acting as a competitive inhibitor of glucose metabolism[12,13]. 2DG enters cells through glucose transporters and disrupts glycolysis by being phosphorylated by hexokinase-2 (HK2) to form 2-deoxy-D-glucose-6-phosphate (2DG-6-P)[14]. Unlike glucose, 2DG-6-P cannot proceed through the glycolytic pathway, leading to an accumulation that effectively inhibits HK2 activity[14]. This accumulation reduces glycolytic ATP production, limiting the energy and metabolites required for the inflammatory response[15]. 2DG has been widely used to explore the role of glycolysis in various diseases[12]. In cancer cell lines, 2DG has been shown to slow cell proliferation and induce apoptosis[16]. Similarly, blocking T-cell glycolysis has been found to prevent graft rejection[17] and reduce excessive IFN-γ production in autoreactive $CD4^+$ T cells[18]. In addition, 2DG has demonstrated the ability to modulate macrophage functions, including cytokine production and phagocytosis[19], and has been implicated in the modulation of several infectious diseases[19]. Moreover, prior studies have shown that high concentrations of 2DG (1 mM) can specifically reduce microglial activity[20], while even higher concentrations (10 mM) can eliminate MG in co-culture models with astrocytes and neurons[21,22].

In this study, we hypothesized that 2DG treatment at lower doses (less than 500 μM) would not only reduce glycolysis but also enhance mitochondrial function and dynamics, promoting a shift from glycolysis to OXPHOS in glial cells (MG and astrocytes). We further posited that this metabolic reprogramming would reduce neuroinflammation. Specifically, we aimed to determine whether 2DG treatment restores mitochondrial activity and bioenergetic profiles in MG and astrocytes and if this restoration decreases pro-inflammatory markers and shifts glial cells toward an anti-inflammatory or regenerative phenotype. We also explored the effects of 2DG on key signaling pathways, such as AMP-activated protein kinase (AMPK), that regulate metabolic and inflammatory responses. Additionally, we evaluated the therapeutic potential of 2DG in mouse models of neuroinflammation, focusing on changes in glial activation, mitochondrial function, and neuroinflammatory markers. Our study revealed that 2DG enhanced OXPHOS, improving mitochondrial membrane potential and restoring mitochondrial morphology. Moreover, we demonstrate that 2DG enhanced spare respiratory capacity, supporting metabolic functions under inflammatory stress. Advanced imaging techniques revealed the protective effects of 2DG on mitochondrial dynamics, adding a novel dimension to its role in combating neuroinflammation. These findings suggest that 2DG represents a promising therapeutic strategy for targeting metabolic dysfunction in neuroinflammatory and neurodegenerative diseases, providing a new avenue for restoring mitochondrial health and mitigating glial-driven neuroinflammation.

Results

Cell polarization and metabolic reprogramming

LPS induces microglia (MG) to polarize into a pro-inflammatory state[23] and astrocytes into a reactive state[24,25], both contributing to heightened neuroinflammation[26,27]. This polarization is coupled with metabolic reprogramming in both cell types, shifting from OXPHOS to glycolysis[28]. Mitochondrial dysfunction ensues, marked by decreased oxygen consumption, impaired mitochondrial membrane potential, disrupted mitochondrial dynamics (fission/fusion imbalance), and reduced mitochondrial biogenesis[29].

LPS-induced changes in glial cell mitochondrial function

We first investigated dose-dependent metabolic alterations induced by various doses of LPS and 2DG in mixed glial cells (MxG) and MG isolated from the mouse brain, with a focus on mitochondrial oxygen consumption rate (OCR) to measure mitochondrial OXPHOS activity. The real-time measurement of OCR was used to assess basal respiration (BR) and spare respiratory capacity (SC) via Seahorse XFe96 Analyzer (Agilent). SC is a measurement of a cell's ability to respond to increased energy demands or stress, which is calculated by subtracting the OCR of BR from the maximal OCR induced by the decoupling agent Carbonyl cyanide 4-trifluoromethoxy-phenylhydrazone (FCCP). A decrease in SC indicates mitochondrial dysfunction or impairment. In MxG, LPS led to a reduction of OCR in BR (at 1 μg/mL) and SC (at 100 ng/mL to 1 μg/mL) after 24 h (Fig. 1a–c). A slight increase in BR and SC was observed when MxG was incubated with 2DG alone at 500 μM and 200 μM for 24 h, respectively (Fig. 1d–f). We repeated the same experiment in purified MG cultures to validate whether this phenomenon can be observed in MG. LPS led to a reduction of OCR in BR (at 500 ng/mL) and in SC (at 100 ng/mL to 500 ng/mL) after 24 h (Fig. 1g–i). However, 2DG alone altered neither BR nor SC in MG (Fig. 1j–l).

2DG mitigated LPS-induced changes in MxG, MG, and BV2 cell metabolism

We tested whether 2DG could reverse the metabolic changes induced by LPS in MxG, MG, and BV2 cells. We incubated the cells for 24 h with LPS (100 ng/mL or 200 ng/mL, which decreased SC in MxG and MG), then we replaced the media with the addition of various doses of 2DG or vehicle for another 24 h prior to extracellular flux analysis by Seahorse assay. 2DG at 200 μM and 500 μM increased SC in LPS-stimulated MxG by almost 2-fold compared to cells treated with LPS (200 ng/mL) + vehicle (Fig. 2a–c) and LPS (100 ng/mL) + vehicle (Fig. S1a–c). In MG, 2DG at 50, 100, and 200 μM ameliorated the metabolic effects of 200 ng/mL LPS and increased both BR and SC after 24 h (Fig. 2f–h). Similar findings were observed in BV2 cells (Fig. S1d–f), as 2DG at 100 μM and 500 μM could reverse the effects of LPS in cells pre-incubated with 100 ng/mL LPS for 24 h.

2DG treatment attenuated the LPS-induced decrease in mitochondrial membrane potential

Mitochondrial membrane potential (MMP) is a vital indicator of mitochondrial health and function, driving ATP production through OXPHOS by maintaining the electrochemical gradient necessary for efficient electron transport and energy generation. A stable MMP is crucial for several mitochondrial functions, including ATP

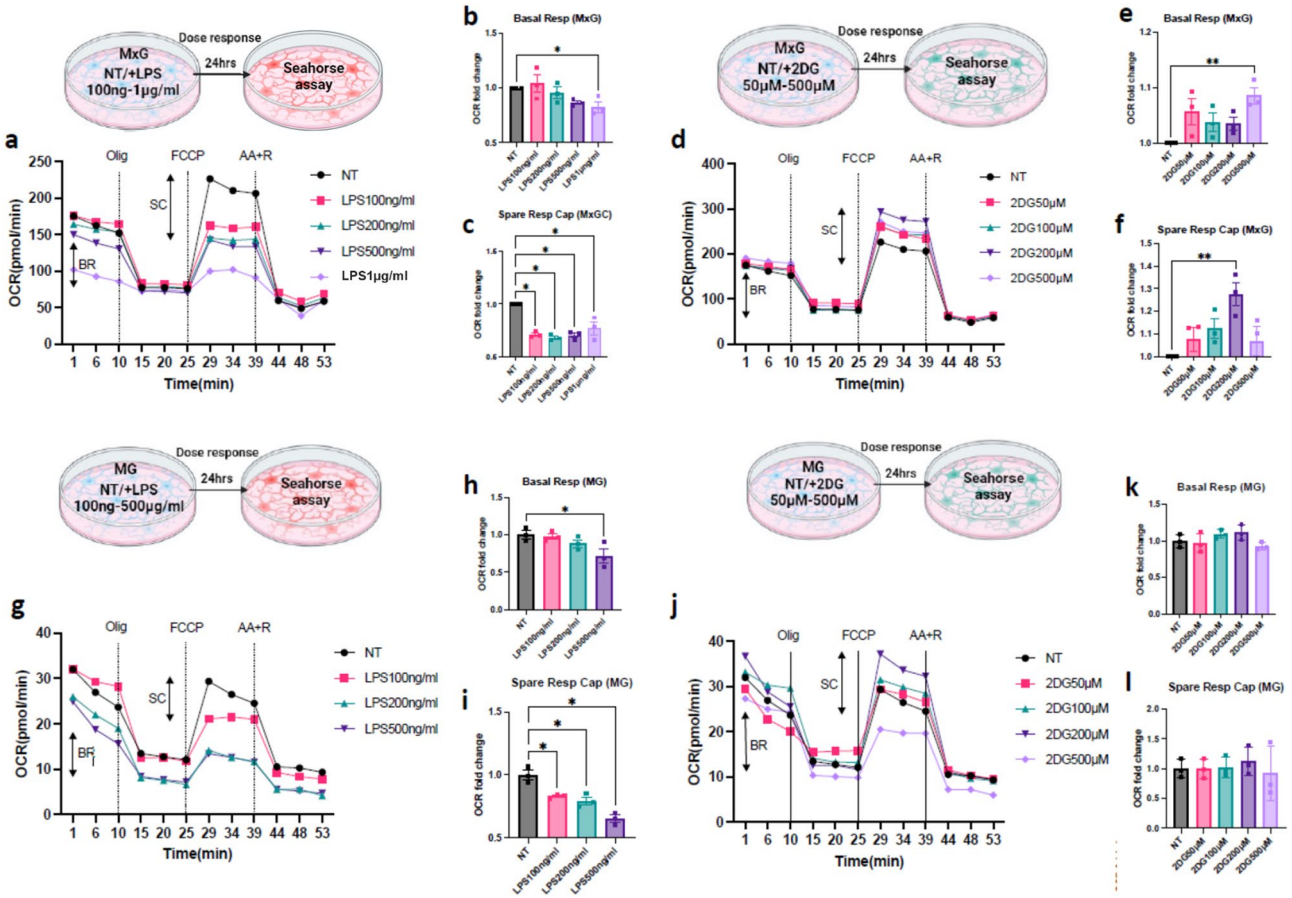

Fig. 1. LPS downregulates OXPHOS in mixed glial cells (MxG) and microglia (MG). A dose-dependent metabolic shift in MxG and MG induced by LPS (**a**–**c** and **g**–**i**, respectively) and 2DG alone (**d**–**f** and **j**–**l**, respectively), measured as oxygen consumption rate (OCR) via Seahorse extracellular flux assay. LPS, lipopolysaccharide; 2DG, 2-Deoxy-D-glucose; FCCP, carbonyl cyanide-4-(trifluoromethoxy)phenylhydrazone; Olig, oligomycin; AA, antimycin a; R, rotenone; NT, no treatment. Seahorse data are derived from 3 independent experiments, each including 3 to 5 biological replicates. Bar graphs are presented as fold change relative to the NT group and are expressed as mean ± SEM. $^{*}p \leq 0.05$, $^{**}p \leq 0.01$, $^{****}p \leq 0.001$, One-way ANOVA with Tukey multiple comparison testing.

synthesis, calcium regulation, and control of reactive oxygen species production. JC-1 dye is commonly used to assess MMP, as it accumulates in mitochondria in a potential-dependent manner. In healthy mitochondria with high membrane potential, JC-1 forms an aggregate that emits red fluorescence, whereas in depolarized mitochondria with reduced MMP, it remains in its monomeric form, emitting green fluorescence. A decreased red/green fluorescence ratio reflects mitochondrial depolarization and dysfunction. Our study demonstrated that 200 ng/mL LPS exposure for 24 h in both MxG and MG disrupted MMP, as evidenced by a reduced red/green fluorescence ratio, indicating mitochondrial depolarization. However, 2DG treatment effectively attenuated this depolarization by increasing the JC-1 red/green fluorescence ratio in both MxG (Fig. 2d,e) and MG (Fig. 2i,j).

Cell polarization and mitochondrial dynamics

Cell polarization in MG and astrocytes involves mitochondrial dynamics, including fission and fusion, that regulate mitochondrial shape, size, and function which is crucial for energy balance[28,30]. Disruptions in these processes can lead to mitochondrial dysfunction and contribute to disease states[29].

2DG treatment attenuated LPS-induced mitochondrial fragmentation

MitoTracker is a fluorescent dye that selectively labels mitochondria, making it an effective tool for studying mitochondrial morphology and dynamics, as it allows visualization of mitochondrial structure, network connectivity, and spatial distribution within cells[31]. For OXPHOS, cells need healthy mitochondria which are generally tubular and exist in complex networks, whereas cells undergoing profound stress often display swollen and fragmented mitochondria, marked by concurrent disruption of metabolism, membrane potential, and Ca^{2+} signaling[32]. Therefore, quantitative imaging-based assessment of mitochondrial morphology and dynamics can provide valuable insights into cellular physiology and pathophysiology. By tracking changes in mitochondrial shape, such as fragmentation or elongation, and assessing dynamic processes like fission and fusion, MitoTracker

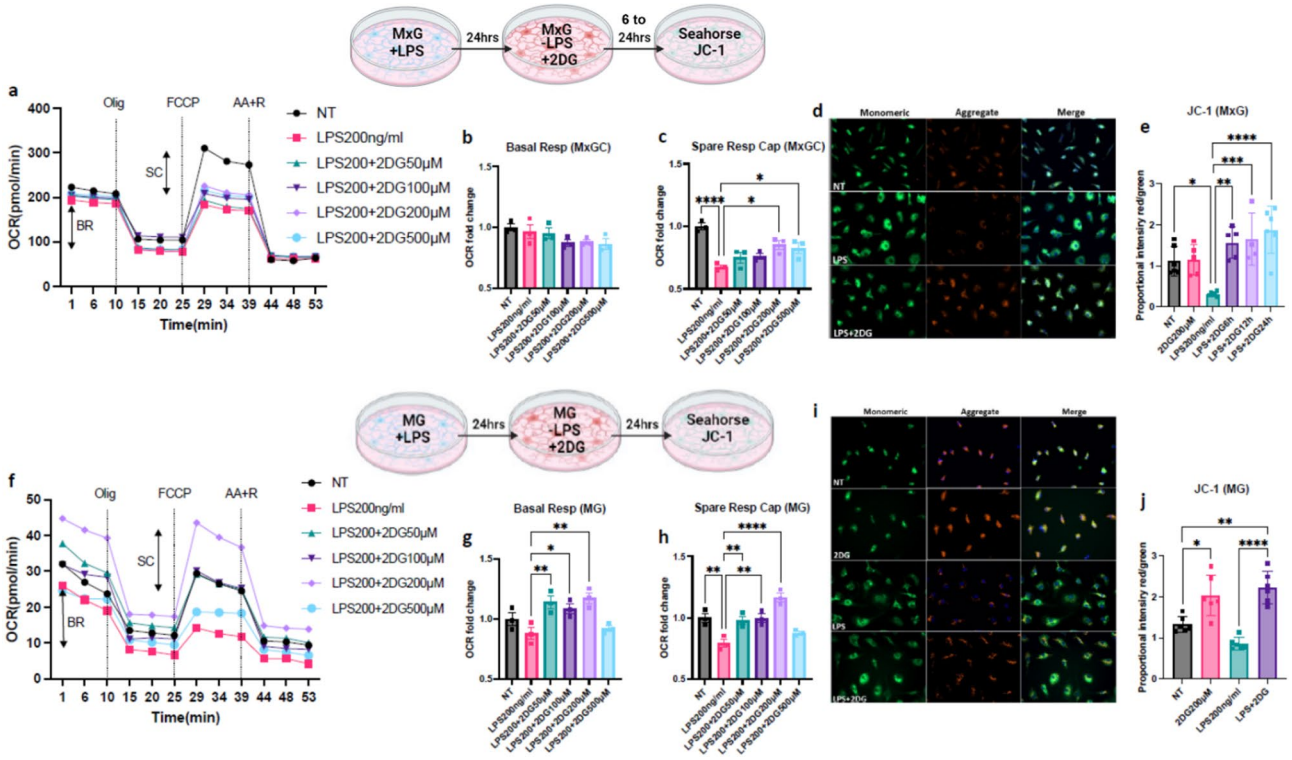

Fig. 2. LPS-induced changes in OXPHOS are reversed by 2DG in mixed glial cells (MxG) and microglia (MG). Cells were stimulated for 24 h with vehicle or LPS (200 ng/mL) followed by treatment with vehicle or 2DG for up to an additional 24 h. Treatment with 2DG at 200 μM and 500 μM for 24 h partially reversed the metabolic shift induced by LPS in MxG (**a**–**c**). Treatment with 2DG at a concentration of 200 μM for 6, 12, and 24 h mitigated the LPS-induced reduction in mitochondrial membrane potential, as assessed by JC-1 dye staining (**d**,**e**). Treatment with 2DG at 100 μM and 200 μM for 24 h effectively reversed the metabolic shift induced by LPS exposure in MG (**f**–**h**). Treatment with 2DG at 200 μM for 24 h improved mitochondrial membrane potential in MG, as evidenced by the increased JC-1 red/green fluorescence ratio (525/565) in both untreated cells and LPS-treated (24 h) cells (**i**,**j**). LPS, lipopolysaccharide; 2DG, 2-Deoxy-D-glucose; OCR, oxygen consumption rate; FCCP, carbonyl cyanide-4-(trifluoromethoxy)phenylhydrazone; Olig, oligomycin; AA, antimycin a; R, rotenone; NT, no treatment. Seahorse data are derived from 3 independent experiments, each including 3 to 5 biological replicates. Quantification of JC-1 staining is derived from a minimum of 5 independent experiments, each including at least six fields per condition. Bar graphs are presented as fold change relative to the NT group and are expressed as mean ± SEM. $^{*}p \leq 0.05$, $^{**}p \leq 0.01$, $^{****}p \leq 0.001$, One-way ANOVA with Tukey multiple comparison testing.

provides insights into mitochondrial health and function. We showed that 200 ng/mL LPS exposure for 24 h in MG disrupted this balance by increasing mitochondrial fragmentation and reducing network connectivity, indicating mitochondrial dysfunction. LPS induced more fragmented mitochondria, as indicated by an increase in their circularity and a reduction in mean area and mean perimeter; however, 2DG could restore these effects (Figs. 3 and S2). In mitochondrial morphology analysis, mean aspect ratio (AR) and mean form factor (FF) are key metrics used to quantify mitochondrial shape[33]. The AR measures the elongation of mitochondria, calculated as the ratio of their length to width, where higher values indicate more elongated mitochondria and lower values suggest rounded or fragmented shapes. The FF assesses the complexity and connectivity of mitochondrial networks, with higher values indicating more elongated and interconnected mitochondria, while lower values reflect fragmentation[33]. Our data showed that the mean of both AR and FF decreased significantly by 200 ng/mL LPS exposure for 24 h in MG, whereas 2DG increased the mean FF, indicating elongated and more highly connected mitochondria. Similarly, 2DG restored LPS-induced changes in mitochondrial branching and mean branch length (Figs. 3 and S2).

2DG treatment upregulated nuclear-encoded mitochondrial biogenesis markers

The data presented above demonstrate that 2DG can prevent LPS-induced mitochondrial fragmentation, increase MMP, and enhance mitochondrial OCR to support OXPHOS in both MxG and MG. These findings prompted us to explore whether 2DG affects the expression of genes and proteins that regulate mitochondrial dynamics, both in vitro and in vivo. Specifically, we investigated how 2DG influences key nuclear-encoded markers involved in mitochondrial biogenesis, fission, and fusion under inflammatory conditions in MxG and LPS-induced neuroinflammation in mice. MxG were incubated with LPS (200 ng/mL) for 24 h, followed by replacement with fresh media containing 2DG (200 μM) or vehicle for an additional 24 h. Our qPCR analysis

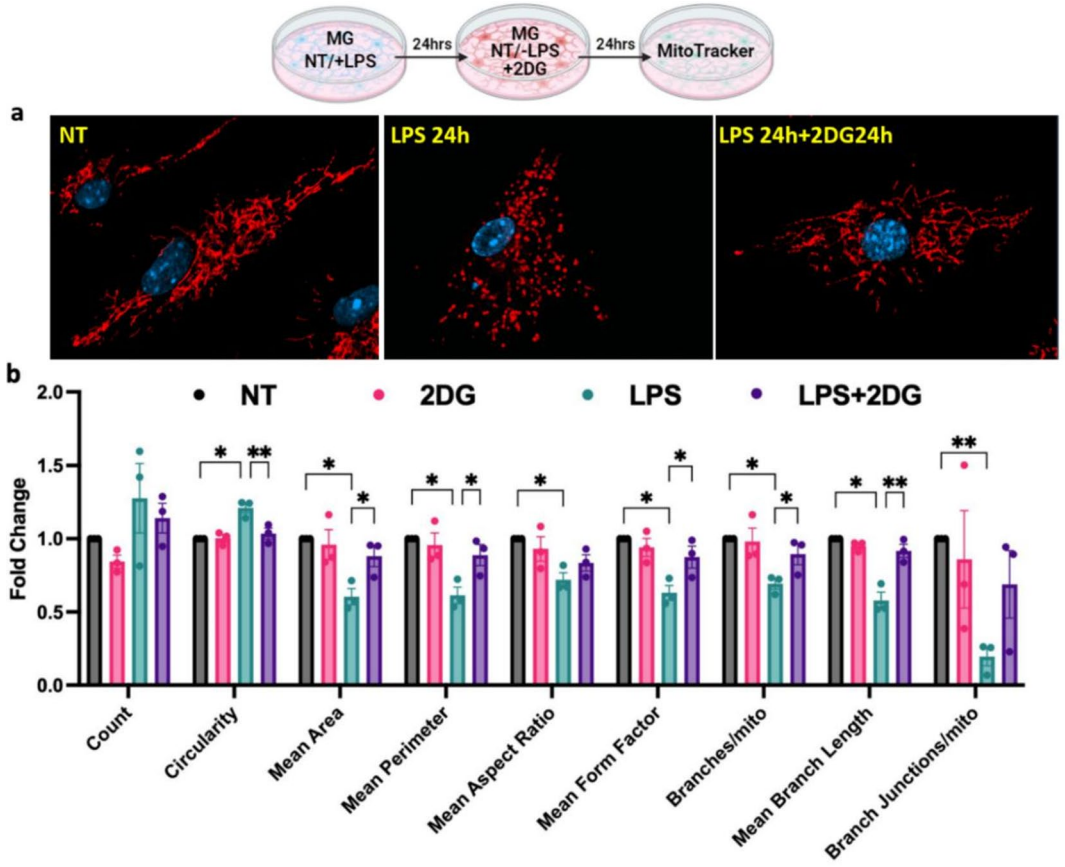

Fig. 3. Treatment with 2DG restores mitochondrial morphology in LPS-stimulated MG. MG were stimulated for 24 h with vehicle or LPS (200 ng/mL) followed by treatment with vehicle or 2DG (200 µM) for an additional 24 h. MitoTracker was used to assess mitochondrial structure and network connectivity (**a**). LPS induced mitochondrial fragmentation with an increase in circularity, decrease in mean aspect ratio and form factor as well as in area and mean perimeter. Moreover, LPS reduced the overall connectivity and morphological complexity of the mitochondrial network quantified by the number of branches per mitochondria, the number of branch junctions, and the mean length of branches. 2DG reversed the LPS-induced morphological and structural changes and restored the filamentous structure of mitochondria (**b**). Data are derived from at least six fields per condition normalized to the NT group (magnification 630×) in 3 independent experiments. LPS, lipopolysaccharide; 2DG, 2-Deoxy-D-glucose; NT, no treatment. Bar graphs expressed as mean ± SEM. $^{*}p \leq 0.05$, $^{**}p \leq 0.01$, One-way ANOVA with Tukey multiple comparison testing.

showed that in the absence of 2DG, LPS-treated MxG exhibited increased expression of *Tfam* and *Mgme2*, with a reduction in *Nrf2* expression. However, 2DG treatment following LPS stimulation led to significant upregulation of *Tfam*, *Mgme2*, *Nrf1*, *Ppargc1a*, *Peo1*, *Polg2*, and *Polrmt* compared to LPS stimulation plus vehicle (Fig. 4a). LPS also elevated the expression of mitofission markers *Drp1* and *Mid51* while downregulating the mitofusion marker *Opa1*. In contrast, 2DG treatment reduced the expression of mitofission markers *Drp1*, *Mff*, *Mid41*, and *Mid51*, while increasing *Opa1* expression as a mitofusion marker (Fig. 4b,c). These findings were further validated by Western blot (InCell Western assay) analysis, showing increased protein levels of TFAM, PGC1α (protein of *Ppargc1a*), and OPA1, and decreased DRP1 expression (Fig. 4d–h).

LPS administration is commonly used to model neuroinflammation in vivo[34,35]. To investigate the effects of 2DG on metabolism and the inflammatory response within the CNS, we utilized two complementary models of LPS-induced neuroinflammation, delivering LPS either systemically through intraperitoneal (ip) injection or directly into the CNS via intracerebroventricular (icv) administration. Brain tissue was then analyzed using qRT-PCR and immunoblotting. In the ip injection model, mice received daily LPS or saline (sham) + 2DG or vehicle by ip administration for 1 week. LPS treatment led to a downregulation of mitochondrial biogenesis markers such as *Nrf1/2*, *Ppargc1a*, *Peo1*, and *Polg2*, as well as most mitofission markers, compared to the sham control group (Fig. 4i,j). Similar findings were observed following icv administration of LPS; in this case, mice were injected once with LPS via icv administration, followed by daily, systemic (ip) treatment with 2DG or vehicle for 1 week. In this model, LPS downregulated all biogenesis, mitofission, and mitofusion markers compared to the sham group (Fig. 4l–n). In both in vivo model systems, 2DG treatment upregulated key biogenesis markers compared to the LPS + vehicle group, including *Mgme2*, *Nrf1/2*, *Ppargc1a*, *Peo1*, and *Polg2* (for ip model) and *Tfam*, *Nrf1*, *Ppargc1a*, and *Polg2* (for icv model). Additionally, 2DG increased the expression of mitofusion

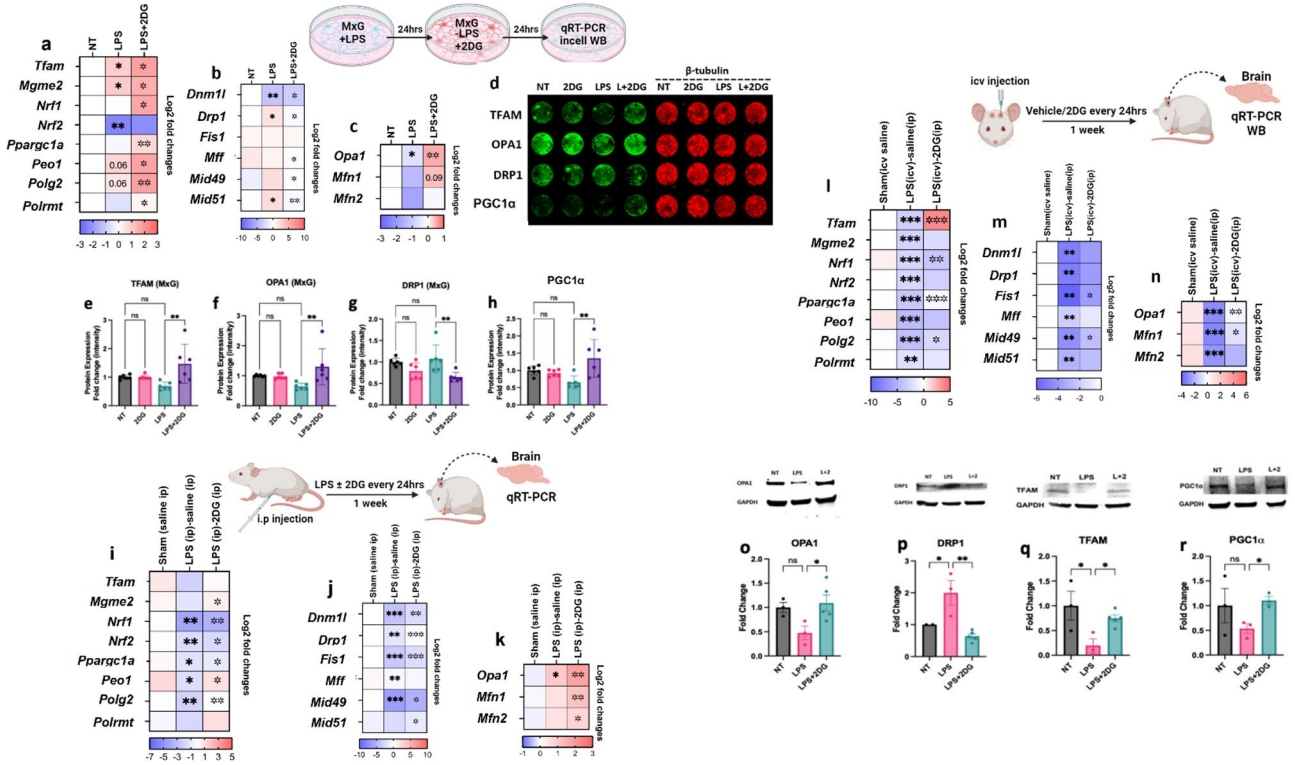

Fig. 4. 2DG upregulates nuclear-encoded mitochondrial biogenesis genes and mitigates the effects of LPS on mitochondrial fission/fusion gene expression, both in vitro and in vivo. Shown are the results of qRT-PCR from MxG (**a**–**c**) and mouse brain following LPS-induced neuroinflammation [intraperitoneal (ip) LPS treatment (**i**–**k**); intracerebroventricular (icv) LPS treatment (**l**–**n**)], with and without 2DG treatment. Protein expression was also analyzed via InCell Western assay in MxG (**d**–**h**) and Western blot from brain tissue in the icv LPS model (**o**–**r**). LPS, lipopolysaccharide; 2DG, 2-Deoxy-D-glucose; NT, no treatment; MxG, mixed glial cells; ip, intraperitoneal; icv, intracerebroventricular; WB, Western blot; ns, not significant. qRT-PCR data are derived from 3 independent experiments, each including a minimum of 3 biological replicates (for MxG) or from 3 independent animals, each including a minimum of 3 technical replicates. Quantification of InCell Western assay is derived from at least 3 independent experiments per group. The quantification of WB is from 3 independent animals. Bar graphs are presented as fold change relative to the NT group and are expressed as mean ± SEM. $^{*}p \leq 0.05$, $^{**}p \leq 0.01$, $^{****}p \leq 0.001$ (for qRT-PCR, solid asterisks refer to LPS vs. NT; hollow asterisks refer to LPS + 2DG vs. LPS), One-way ANOVA with Tukey multiple comparison testing.

genes *Opa1* and *Mfn1/2* (ip) and *Opa1* and *Mfn1* (icv) in both models (Fig. 4k,n). Immunoblotting confirmed that 2DG enhanced the protein expression of OPA1, TFAM, and PGC1α while reducing DRP1 expression (Fig. 4o–r).

2DG treatment upregulated nuclear- and mitochondrial-encoded bioenergetic markers

Our results suggested that 2DG stimulates mitochondrial biogenesis, prompting us to explore whether 2DG also modulates bioenergetic markers linked to mitochondrial energy production (particularly OXPHOS) in MxG and LPS-induced neuroinflammation in mice. In MxG, LPS treatment reduced the expression of mitochondrial-encoded genes related to electron transport chain complexes, including complex-I (*Nd2-Nd5*), complex-IV (*Cox1&2*, *Mt-Co2 and Mt-Co3*), and complex-V (*Atp6* and *Atp8*), compared to untreated cells as measured by qRT-PCR. However, 2DG treatment rescued this effect, significantly upregulating these genes compared to the LPS + vehicle group (Fig. 5a). Furthermore, 2DG induced the overexpression of the nuclear-encoded complex-I gene, *Ndufb8*, compared to the LPS + vehicle group (Fig. 5b). These findings were validated by InCell Western analysis, which showed increased protein levels of Cytochrome-C (CytC; complex-III) and MTCO2 (complex-IV) (Fig. 5c–e).

In our in vivo studies, mice treated with LPS (ip or icv) plus saline for one week showed downregulation of both nuclear- and mitochondrial-encoded bioenergetic markers compared to sham-treated mice. Interestingly, 2DG treatment upregulated these markers in both in vivo models (Fig. 5f–i). WB from the samples of the mice treated with LPS (icv) further confirmed that 2DG increased the protein expression of the nuclear-encoded bioenergetic marker NDUFB8 (complex-I or CI) as well as SDHB, ATP5A, and UQCRC2, proteins involved in complexes-II, -V, and -IV, respectively (Fig. 5j–n).

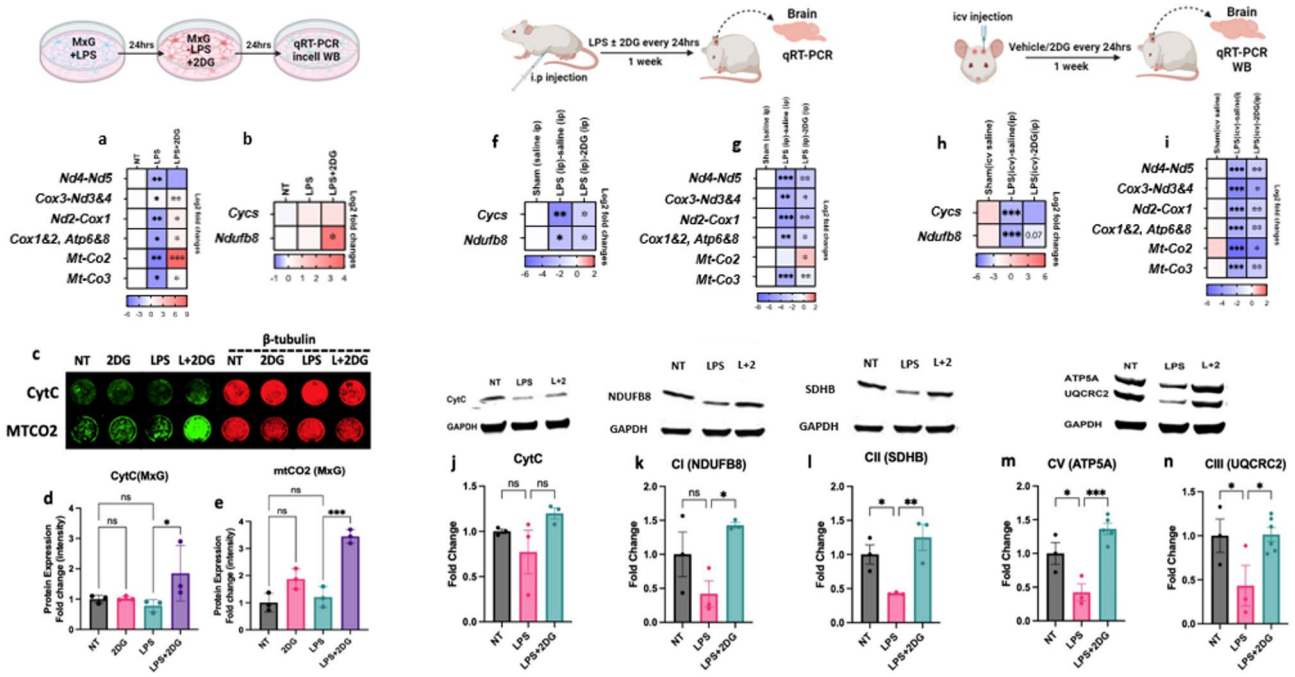

Fig. 5. 2DG mitigates the downregulation of nuclear- and mitochondrial-encoded bioenergetic gene expression induced by LPS, both in vitro and in vivo. Shown are results from MxG (**a**,**b**: qRT-PCR; **c**–**e**: InCell Western assay) and mouse brain following intraperitoneal (**f**,**g**: qRT-PCR) and intracerebroventricular (**h**,**i**: qRT-PCR; **j**–**n**: Western blot) LPS injection. LPS, lipopolysaccharide; 2DG, 2-Deoxy-D-glucose; NT, no treatment; MxG, mixed glial cells; ip, intraperitoneal; icv, intracerebroventricular; WB, western blot; ns: not significant; CytC, cytochrome-c; CI, II, III, IV, mitochondrial complex I, II, III, IV. qRT-PCR data are derived from 3 independent experiments, each including a minimum of 3 biological replicates (for MxG) or from 3 independent animals, each including a minimum of 3 technical replicates. Quantification of InCell Western assay is derived from 3 independent experiments, each including a minimum of 3 biological replicates. Quantification of WB is from 3 or more independent animals per group. Bar graphs are presented as fold change relative to the NT group and are expressed as mean ± SEM. $^{*}p \leq 0.05$, $^{**}p \leq 0.01$, $^{****}p \leq 0.001$, ns: not significant (for qRT-PCR, solid asterisks refer to LPS vs. NT; hollow asterisks refer to LPS + 2DG vs. LPS), One-way ANOVA with Tukey multiple comparison testing.

Cell polarization and inflammatory response

LPS drives MG into a pro-inflammatory state and astrocytes into a reactive state, both contributing to increased neuroinflammation[36]. Metabolic reprogramming from an OXPHOS-dominant to a glycolytic state has been associated with the downstream inflammatory effects of LPS[37]. Since we found that 2DG rescues LPS-induced effects on OXPHOS and mitochondrial dynamics in MxG and MG, we next explored whether 2DG can modulate inflammatory signaling both in vitro and in vivo.

LPS-induced polarization did not alter cell viability in MxG

Before investigating the effects of 2DG on inflammatory markers in vitro, we first assessed the impact of LPS (200 ng/mL), 2DG (200 µM), and LPS + 2DG, doses selected based on the Seahorse assay (Figs. 1 and 2), on cell viability. InCell Western analysis using Sapphire-700 staining showed that 24-h incubation with LPS, 2DG, or LPS + 2DG did not affect cell viability (Fig. S3).

2DG treatment modulated inflammatory markers in vitro

Gene expression analysis by qRT-PCR showed that LPS (200 ng/mL) treatment of MxG for 24 h induced the expression of inflammatory markers such as *Aif1*, *Nos2*, *Tnf*, and *Il6* while downregulating the alternative activation markers *Il4*, *Il10*, and *Arg1* (Fig. 6a). However, an additional 24-hour treatment with 2DG (200 µM) reversed these effects, downregulating *Aif1*, *Nos2*, *Tnf*, and *Il6*, and upregulating *Il4*, *Il10*, and *Arg1*. InCell Western analysis confirmed that 2DG reduced the protein levels of Iba1, iNOS, and TNFα while increasing Arg1 expression in MxG. Notably, 2DG alone also decreased the protein expression of Iba1 and TNFα and increased Arg1, even without prior LPS treatment (Fig. 6b–f).

Immunocytochemistry (ICC) of isolated MG also revealed that LPS increased the number of Iba1 and iNOS-positive cells after 24 h, compared to untreated cells. However, 2DG treatment for an additional 12 h reduced the number of Iba1 and iNOS-positive cells in LPS-treated MG compared to cells not treated with 2DG. While Arg1-positive cells showed no change after 12 h, 2DG incubation for 24 h increased the number of Arg1-positive cells without affecting Iba1 levels (Fig. 6g–l).

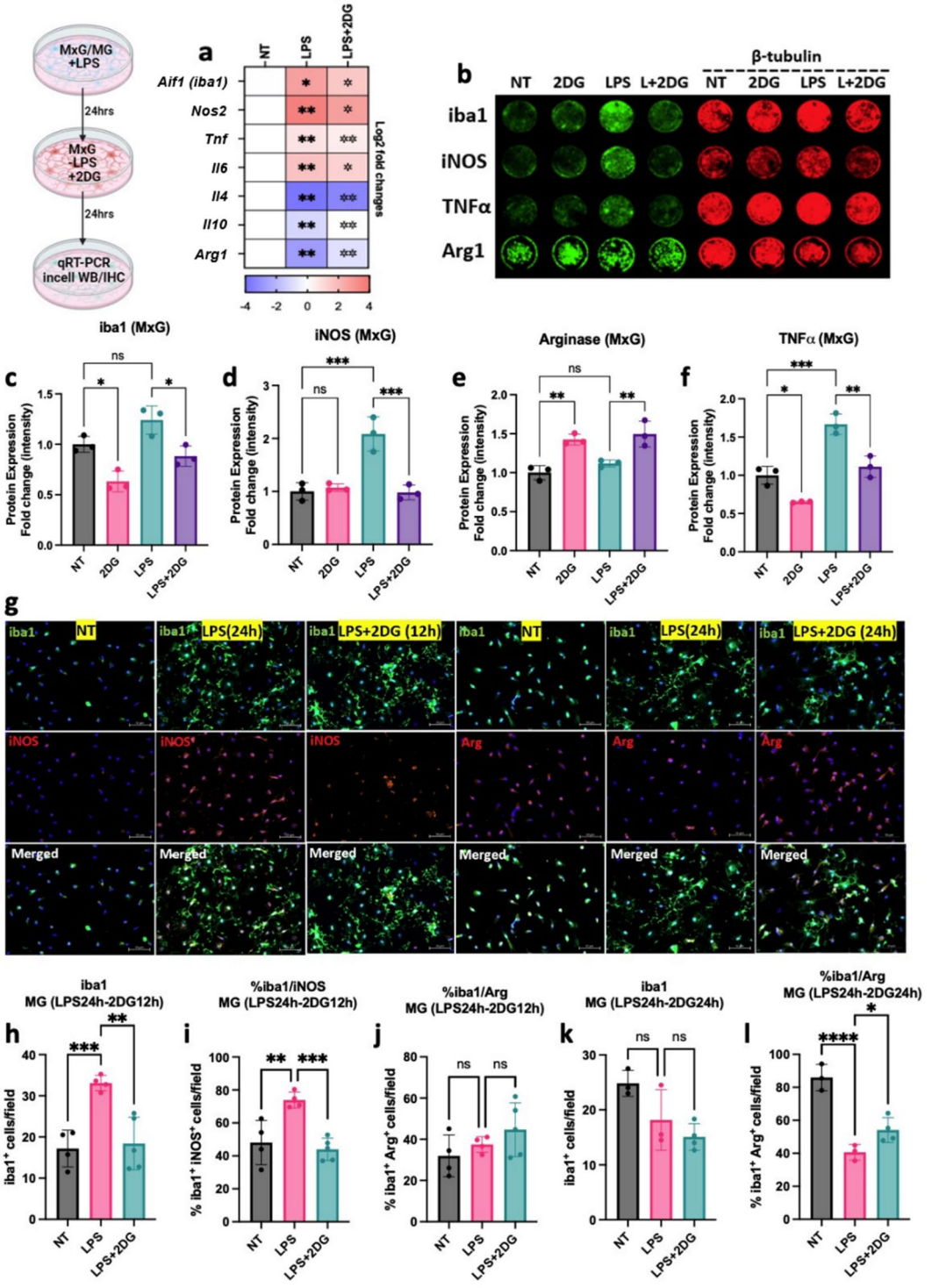

Fig. 6. 2DG reverses the effect of LPS on inflammatory gene expression in MxG and MG. MxG were treated with LPS (200 ng/mL) for 24 h followed by vehicle or 2DG (200 μM) for 24 h (**a:** qRT-PCR and **b**–**f**: InCell Western assay). In other experiments, MG were treated with LPS (200 ng/mL) for 24 h then vehicle or 2DG (200 μM) was added for 12 and 24 h followed by staining for inflammatory markers by immunocytochemistry (**g**–**l**). LPS, lipopolysaccharide; 2DG, 2-Deoxy-D-glucose; NT, no treatment; MxG, mixed glial cells; MG, microglia; ns, not significant; Arg1, arginase-1. qRT-PCR data are derived from 3 independent experiments, each including a minimum of 3 biological replicates. Quantification of InCell Western assay and IHC is derived from a minimum of 3 independent experiments, each including at least 3 biological replicates. Bar graphs are presented as fold change relative to the NT group in InCell Western assay and are expressed as mean ± SEM. For immunocytochemistry, bar graphs are the number of the cells per field or percentage of double positive cells. $^{*}p \leq 0.05$, $^{**}p \leq 0.01$, $^{***}p \leq 0.001$ (for qRT-PCR, solid asterisks refer to LPS vs. NT; hollow asterisks refer to LPS + 2DG vs. LPS), One way ANOVA with Tukey multiple comparison testing.

One major component of MxG is astrocytes. LPS activates astrocytes, triggering a reactive response characterized by the release of pro-inflammatory cytokines (e.g., TNFα, IL-1β, IL-6) and inducing a metabolic shift from OXPHOS to glycolysis to meet the energy demands of inflammation, thereby amplifying neuroinflammation. A1 and A2 astrocytes represent two distinct reactive states in vitro, with A1 astrocytes shown to play pro-inflammatory and neurotoxic roles[38]. Our qRT-PCR results showed that LPS (200 ng/mL) for 24 h followed by vehicle for additional 24 h increased A1 astrocytic markers (*Gbp2*, *Psmb8*, *C3*, *Iigp2*, *Lcn2*, *Amigo*, *H2-T23*) and downregulated A2 markers (*Clcf1*, *Tm4sf1*, *Cd109*, *Ptgs2*) in MxG. However, 2DG treatment for an additional 24 h mitigated these effects, downregulating A1 markers (*Lcn2*, *amigo*) and upregulating A2 markers (*Clcf1*, *Cd109*, *Ptgs2*) compared to LPS followed by vehicle treatment (Fig. S4).

2DG treatment modulated inflammatory markers in vivo

In our in vivo studies, mice treated with LPS + saline (ip) for one week showed increased *Tnf* and decreased *Il6*, *Il4*, *Il10*, and *Arg1* levels in their brains, as measured by qRT-PCR. Conversely, mice treated with LPS + 2DG (ip) exhibited reduced *Nos2* and *Tnf* expression and increased levels of *Aif1*, *Il6*, *Il4*, *Il10*, and *Arg1* compared to those not treated with 2DG (Fig. 7a). In a separate experiment, mice administered LPS (icv) followed by saline (ip) for one week had elevated *Nos2* and *Tnf* and reduced *Aif1*, *Il6*, *Il4*, *Il10*, and *Arg1*. However, mice treated with 2DG (ip) for one week showed lower *Nos2* and higher *Aif1*, *Il6*, *Il4*, and *Arg1* levels compared to those not treated with 2DG (Fig. 7b). WB analysis of brains confirmed that 2DG treatment decreased the protein expression of Iba1, TNFα, and COX2 while increasing Arg1 in mice with neuroinflammation induced by LPS (icv) (Fig. 7c–g).

2DG treatment modulated scavenging phenotypes and phagocytosis

Regenerative or anti-inflammatory microglia are marked by increased phagocytic activity that supports tissue repair and inflammation resolution[39]. Our findings indicate that 2DG can shift the inflammatory response induced by LPS from a pro-inflammatory to an anti-inflammatory state in MxG (MG and astrocytes). We investigated whether 2DG also influences scavenging phenotypes and functional phagocytosis in MxG and MG, respectively. qPCR revealed that LPS (200 ng/mL) downregulated key scavenger genes such as *Cd36*, *Marco*, *Fcrls*, *Cxcl16*, *Cd163*, and *Axl*, while 2DG (200 µM) mitigated this effect, upregulating these genes and others like *Ch25h*, *Clec7a*, *P2y6r*, *Scrab1*, *Stab1*, and *Trem2* compared to LPS + vehicle (Fig. 8a). InCell Western assay further confirmed increased expression of CD206 and Galectin-3 in 2DG-treated MxG, indicating enhanced scavenging activity (Fig. 8b–d). Additionally, functional phagocytosis assays showed that 2DG increased phagocytic uptake of fluorescently tagged myelin in LPS-stimulated MG (Fig. 8e,f).

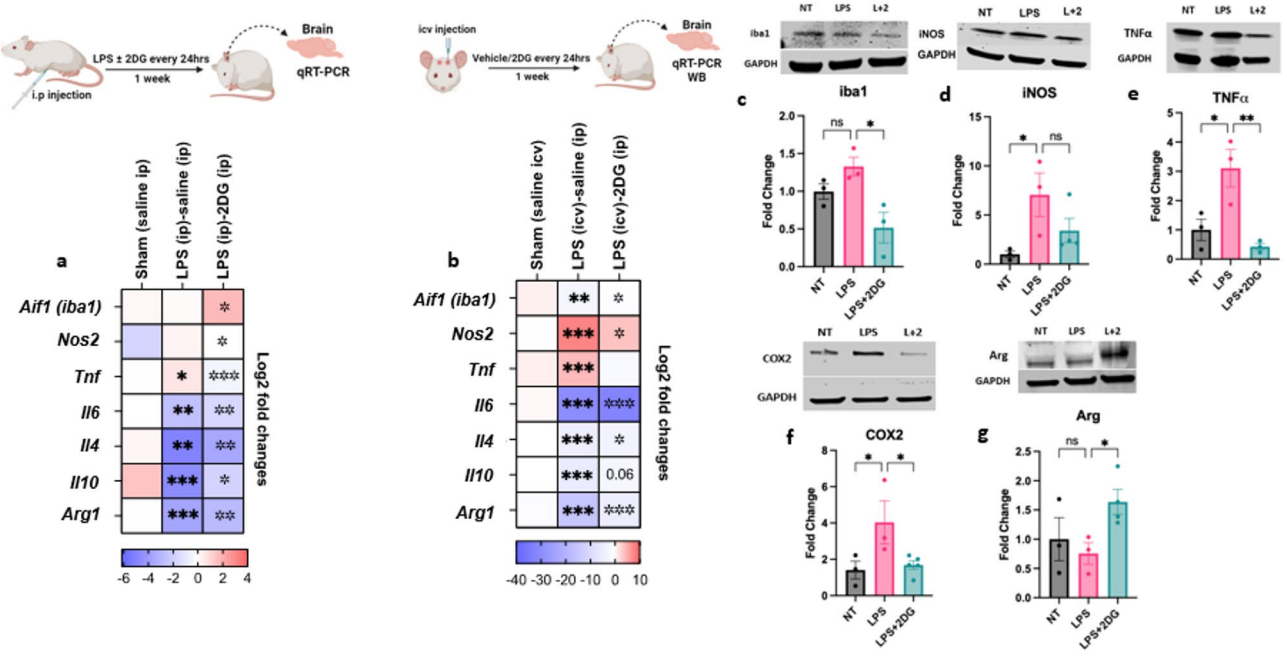

Fig. 7. 2DG modulates inflammatory gene expression in LPS-induced neuroinflammation in the brain. Expression of inflammatory markers was evaluated from the mouse brain following intraperitoneal (**a**: qRT-PCR) and intracerebroventricular (**b**: qRT-PCR and **c**–**g**: Western blot) LPS injection ± treatment with 2DG. LPS, lipopolysaccharide; 2DG, 2-Deoxy-D-glucose; NT, no treatment; ns, not significant; Arg, arginase; ip, intraperitoneal; icv, intracerebroventricular. qRT-PCR data are derived from 3 animals, each including a minimum of 3 technical replicates. Quantification of WB is derived from at least 3 animals per group. Bar graphs are presented as fold change relative to the NT group and are expressed as mean ± SEM. $^{*}p \leq 0.05$, $^{**}p \leq 0.01$, $^{***}p \leq 0.001$ (for qRT-PCR, solid asterisks refer to LPS vs. NT; hollow asterisks refer to LPS + 2DG vs. LPS), One-way ANOVA with Tukey multiple comparison testing.

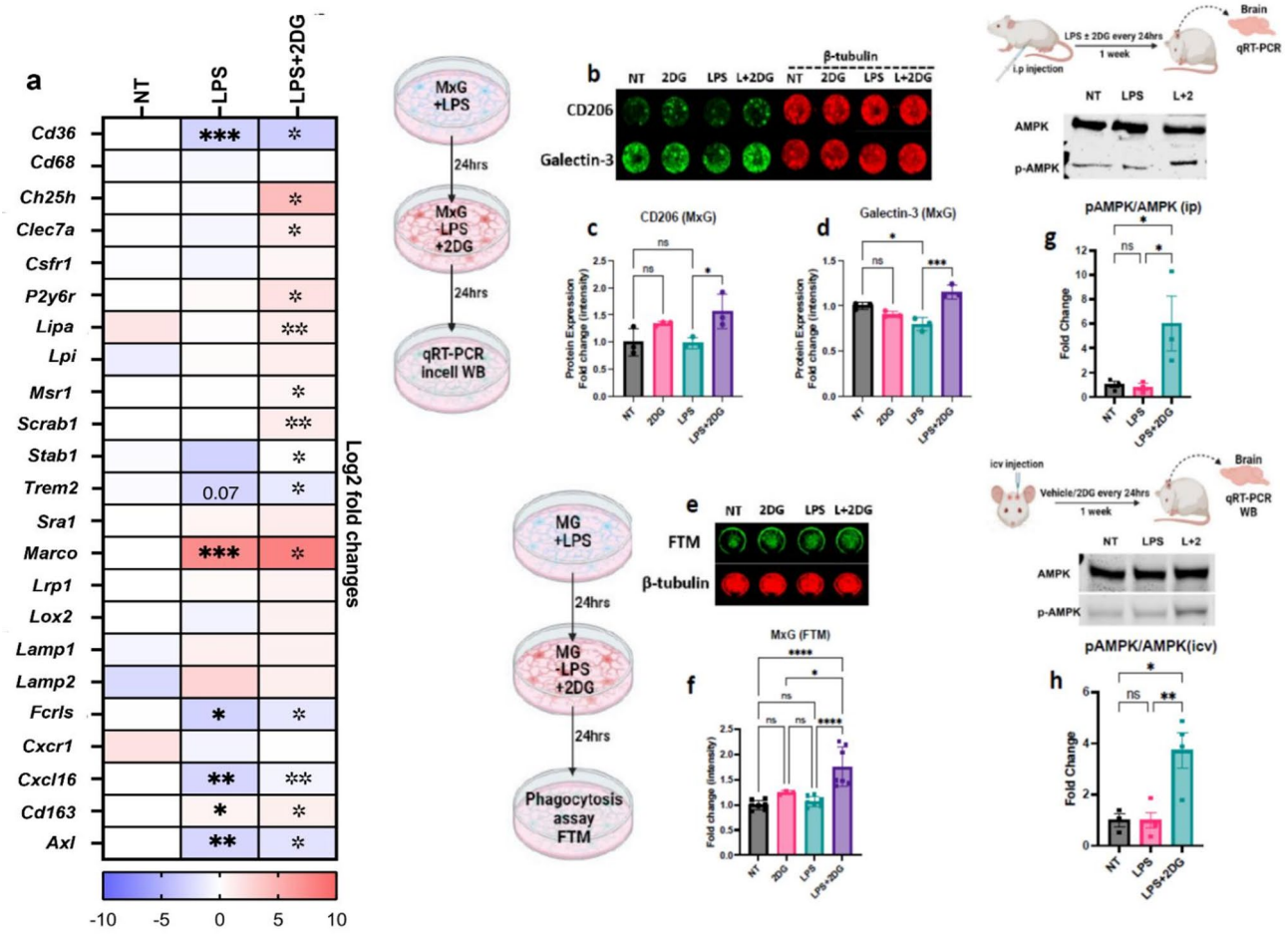

Fig. 8. 2DG modulates scavenging markers and phagocytosis following LPS treatment, both in vitro and in vivo. LPS downregulated scavenging markers in MxG (**a**: qRT-PCR and **b**–**d**: InCell Western assay). 2DG mitigated the effect of LPS on these scavenging markers and led to increased expression of CD206 and Galectin-3 proteins (**b**–**d**). In MG, 2DG increased functional phagocytosis of fluorescent-tagged myelin (**e**,**f**). 2DG increased phosphorylation of AMPK in the brains of animal models of intraperitoneally (**g**: Western blot) and intracerebroventricularly (**h**: Western blot) injected LPS-induced neuroinflammation. LPS, lipopolysaccharide; MxG, mixed glial cells; MG, microglia; 2DG, 2-Deoxy-D-glucose; NT, no treatment; ns, not significant; ip, intraperitoneal; icv, intracerebroventricular; WB, western blot; FTM, fluorescent tagged myelin; L + 2, LPS + 2DG. qRT-PCR data are derived from 3 independent experiments, each including a minimum of 3 biological replicates. Quantification of InCell Western assay, phagocytosis assay and WB are derived from at least 3 independent experiments or animals. Bar graphs are presented as fold change relative to the NT group and are expressed as mean ± SEM. $^{*}p \leq 0.05$, $^{**}p \leq 0.01$, $^{***}p \leq 0.001$ (for qRT-PCR, solid asterisks refer to LPS vs. NT; hollow asterisks refer to LPS + 2DG vs. LPS), One way ANOVA with Tukey multiple comparison testing.

2DG and mitochondrial bioenergetics in LPS-induced inflammation in vivo

Measuring mitochondrial function in vivo after 2DG treatment is essential to determine whether observed increases in mitochondrial markers translate into enhanced bioenergetic performance in the living brain to explore whether 2DG's effects are not solely due to mitochondrial biogenesis or protein expression changes but reflect genuine improvements in metabolic capacity under physiological conditions.

2DG restores LPS-induced mitochondrial dysfunction by enhancing spare respiratory capacity and complex-V activity in isolated brain mitochondria

To determine whether systemic 2DG treatment can preserve or improve mitochondrial function under neuroinflammatory conditions, we examined the bioenergetic profile of brain mitochondria isolated from mice subjected to repeated LPS injections with or without co-administration of 2DG. Isolated mitochondria were analyzed using Seahorse XF extracellular flux analysis to assess OCR across sequential inhibitor/uncoupler additions (Fig. S5). LPS treatment did not significantly alter basal respiration (Fig. S5a,b) but caused a marked reduction in spare respiratory capacity compared with sham controls (Fig. S5c). Co-treatment with 2DG significantly restored spare respiratory capacity close to sham levels, suggesting improved mitochondrial resilience under stress conditions. Consistent with these findings, biochemical assessment of complex-V (ATP

synthase) activity revealed that LPS exposure reduced enzymatic activity relative to sham controls, with a strong trend toward significance ($p = 0.08$; Fig. S5d). Administration of 2DG significantly enhanced complex-V activity compared with LPS alone, indicating that 2DG may support ATP-generating capacity under inflammatory challenge.

2DG showed no effects on mitochondrial oxidative stress

To determine whether these bioenergetic changes were linked to alterations in mitochondrial oxidative stress, we measured ROS/RNS production using a fluorescence-based assay. Neither LPS nor 2DG significantly altered ROS/RNS levels in brain mitochondria isolated from mice (Fig. S5e), suggesting that the observed 2DG-mediated improvements in respiration and ATP synthase activity were not secondary to changes in bulk oxidative stress.

2DG and the activity of AMPK

Our results demonstrated that 2DG modulated MG and MxG cellular metabolism (restoring mitochondrial dynamics and enhancing OXPHOS) and reduced the inflammatory response while shifting cells from a pro-inflammatory to a regenerative state. A potential downstream mechanism of glycolytic inhibition with 2DG could be reduced ATP synthesis leading to activation of the AMPK pathway[40]. Activated AMPK, through phosphorylation, regulates mitochondrial dynamics via the master regulator PGC1α[41] and suppresses inflammation by inhibiting nuclear factor kappa-light-chain-enhancer of activated B cells (NF-κB)[42]. WB analysis of mouse brains from our in vivo experiments confirmed that 2DG induced the pAMPK pathway by increasing phosphorylated AMPK in comparison to mice treated with LPS (ip or icv) + vehicle (Fig. 8g,h).

2DG and autophagy

Neuroinflammation and autophagy are interconnected processes that manage the increased burden of damaged cellular components, such as impaired mitochondria[43]. Autophagy helps maintain cellular homeostasis and counteracts inflammation-induced damage. However, when autophagy is impaired, it can worsen neuroinflammation and contribute to neurodegenerative disease. Using qPCR, our in vivo data revealed that LPS administration reduced the expression of key autophagy-related factors, including *Pink1*, *Park2*, *Map1lc3b*, and *Mapk8* (*Jnk1*), in models of neuroinflammation induced by either ip or icv administration of LPS. Notably, treatment with 2DG reversed these effects, indicating an increase in autophagy (Fig. S6).

Discussion

Neuroinflammation is a key feature of many neurodegenerative diseases, driven by activated MG and astrocytes[44]. With altered metabolic states, these cells play a critical role in shaping the inflammatory response, often exacerbating neuroinflammatory cascades[45]. Our study explored the metabolic reprogramming and mitochondrial dysfunction in neuroinflammation induced by LPS and assessed the potential for 2DG to mitigate these alterations. Higher doses of 2DG potently inhibit glycolysis and can cause broad metabolic suppression and cytotoxicity in certain contexts[46]. These effects are particularly pronounced in highly metabolically active cells, such as cancer cells, which rely heavily on glycolysis for energy production and survival (Warburg effect)[46]. To balance efficacy and safety in neuroinflammation, we selected a low dose (100 mg/kg) guided by literature showing that 100–200 mg/kg modulates metabolism without overt toxicity[47–49]. Higher doses (≥ 500 mg/kg) have been associated with systemic toxicity, including hypoglycemia and weight loss[50], which could confound outcomes in neuroinflammatory models. This strategy aimed to modulate glial glycolysis while preserving homeostatic and reparative functions and minimizing off-target stress. Additionally, lower doses minimize off-target effects and allow for a more nuanced investigation of 2DG's impact on specific pathways, such as the AMPK and autophagy-related pathways, which are critical in modulating inflammation and cellular stress responses. This balance is essential for exploring 2DG's therapeutic potential in neuroinflammatory conditions without compromising the viability or functional integrity of neural and glial cells.

While previous studies have explored the anti-inflammatory effects of modulating glycolysis[51–54], our study provides new insights by directly linking 2DG-induced glycolytic inhibition to improvements in mitochondrial dynamics, including enhanced membrane potential, upregulated fusion and biogenesis markers, and suppression of mitophagy-associated proteins. Additionally, we show that 2DG improves phagocytic function and reprograms glial metabolism toward OXPHOS, which are key components in resolving inflammation and promoting tissue repair. Importantly, our findings were validated both in vitro and in two in vivo models of neuroinflammation, providing translational relevance. Thus, our work extends beyond prior studies by highlighting mitochondrial resilience and phagocytosis as functional outcomes of glycolytic modulation in glia. One of the key findings of this study was that LPS-induced inflammation in MxG and MG was associated with a shift to glycolysis, a well-documented hallmark of activated immune cells[20]. This metabolic shift is known to support rapid cell proliferation and cytokine production at the cost of mitochondrial function. Our data showed that LPS reduces mitochondrial oxygen consumption rate, particularly basal respiration and spare respiratory capacity, indicating an impaired mitochondrial function in both MxG and MG. These findings align with prior research demonstrating that inflammatory stimuli, such as LPS, induce mitochondrial dysfunction by disrupting mitochondrial dynamics, reducing mitochondrial membrane potential and altering mitochondrial morphology[29,55,56]. One of the most compelling results from our study is the ability of 2DG to mitigate these metabolic changes and mitochondrial disruptions. The glycolytic inhibitor 2DG, which mimics glucose deprivation, appears to rescue mitochondrial function by preventing or reversing the LPS-induced metabolic shift.

While 2DG inhibits glycolysis at the level of hexokinase, this can impact cellular ATP production, particularly in highly glycolytic cells[14]. In our study, we observed that mitochondrial respiration and membrane potential were preserved or improved with 2DG treatment, suggesting that energy homeostasis was at least partially maintained through enhanced OXPHOS. However, the inhibition of glycolysis may also influence the pentose

phosphate pathway, which branches from glycolysis and is essential for producing NADPH and maintaining redox balance via glutathione (GSH). A reduction in NADPH could theoretically impair antioxidant capacity and biosynthesis pathways. That said, low-to-moderate doses of 2DG do not deplete ATP significantly and may even increase mitochondrial ATP production due to metabolic reprogramming toward OXPHOS[57]. Although we did not directly measure ATP, NADPH, or GSH levels in this study, future work should assess how 2DG impacts these metabolic intermediates in glial cells under neuroinflammatory conditions to ensure metabolic safety and redox balance are preserved.

Notably, 2DG alone (without pre-exposure of cells to LPS) could enhance mitochondrial respiration in MxG; still, it did not significantly affect the OCR of purified MG alone, suggesting a major role of astrocytes in mixed glia in the resting state. The fact that 2DG reversed the mitochondrial dysfunction induced by LPS in MxG and MG supports the notion that targeting metabolic pathways might offer a therapeutic strategy for diseases marked by glial activation, such as Alzheimer's and multiple sclerosis.

Another significant observation was the restoration of mitochondrial dynamics in LPS-treated MG following 2DG treatment. While LPS induced mitochondrial fragmentation, a hallmark of cellular stress, 2DG reversed this phenomenon by promoting mitochondrial elongation and improving network connectivity. This result is important since mitochondrial fragmentation has been linked to inflammation in neuroinflammatory diseases[11,29,56]. The upregulation of mitochondrial fusion markers such as *Opa1* and *Mfn1*, alongside a downregulation of fission markers like *Drp1*, suggests that 2DG might enhance mitochondrial fusion and stability, further supporting its potential as a therapeutic agent. In addition to its effects on mitochondrial dynamics, 2DG treatment also upregulated key markers of mitochondrial biogenesis, including TFAM, *Ppargc1a* (PGC1α), and *Polg2*, in both in vitro and in vivo models of LPS-induced neuroinflammation. This finding is significant because mitochondrial biogenesis plays a central role in maintaining cellular energy homeostasis[58], and the failure of mitochondrial biogenesis is often observed in neurodegenerative diseases. To directly address whether the increase in mitochondrial bioenergetic markers following low-dose 2DG administration reflects a true enhancement of mitochondrial functional capacity rather than solely an increase in mitochondrial biogenesis, we conducted additional experiments assessing mitochondrial respiration and complex-V activity in isolated brain mitochondria from treated mice. Using Seahorse analysis, we observed a significant elevation in spare respiratory capacity, confirming that 2DG treatment enhances mitochondrial bioenergetic function in vivo. Furthermore, an enzymatic activity assay of mitochondrial complex-V demonstrated increased activity, supporting the notion that 2DG augments intrinsic mitochondrial function in addition to promoting biogenesis. These findings strengthen our conclusion that the bioenergetic improvements induced by low-dose 2DG are attributable to both an increased number of mitochondria and enhanced efficiency of individual mitochondria, highlighting its potential as a metabolic modulator in the CNS.

While our study shows that 2DG improves mitochondrial bioenergetics and reduces inflammatory markers in glial cells, we also begin to uncover the underlying signaling mechanisms. Our data indicates that 2DG activates the AMPK pathway, as shown by increased phosphorylation of AMPK, and upregulates PGC-1α expression, a known co-activator of mitochondrial biogenesis and regulator of anti-inflammatory gene expression. AMPK activation is known to inhibit NF-κB signaling[42], thereby reducing transcription of pro-inflammatory cytokines. Because NF-κB can antagonize NRF2 activity by upregulating KEAP1 or competing for transcriptional coactivators[59], suppression of NF-κB by 2DG may secondarily stabilize and activate NRF2. NRF2 is a master regulator of antioxidant responses, controlling the expression of genes involved in glutathione synthesis, NADPH production, and redox homeostasis[60]. Thus, the observed bioenergetic improvements and reduced inflammatory tone in 2DG-treated glia may be explained, at least in part, by an AMPK-NF-κB-NRF2 signaling axis. This integrated mechanism suggests that 2DG not only reprograms cellular metabolism toward oxidative phosphorylation but also promotes a redox-protective, anti-inflammatory phenotype. Future studies employing specific pathway inhibitors and genetic knockdowns will be needed to confirm the relative contributions of AMPK, NF-κB, and NRF2 to these beneficial effects. An important limitation of this study is the absence of cytosolic and mitochondrial calcium measurements. Calcium uptake into mitochondria is a critical regulator of several dehydrogenases in the TCA cycle and thus directly influences ATP production. In neuroinflammatory settings, dysregulated calcium handling may impair mitochondrial function and exacerbate glial activation. Although we observed improvements in mitochondrial respiration and membrane potential following 2DG treatment, it remains unclear whether these effects are accompanied by alterations in calcium dynamics. Future studies incorporating calcium-sensitive dyes (e.g., Rhod-2 AM for mitochondrial Ca^{2+}) or genetically encoded calcium indicators will be useful to further define the impact of 2DG on mitochondrial bioenergetics in the context of inflammation. While our findings demonstrate that 2DG modulates mitochondrial dynamics, restores bioenergetic function, and attenuates the inflammatory phenotype in glial cells, we recognize that the molecular mechanisms underlying these effects remain complex and multifactorial. The observed upregulation of mitofusion markers, increase in mitochondrial membrane potential, and suppression of pro-inflammatory gene expression suggest a metabolic reprogramming favoring oxidative phosphorylation. However, we caution that these results, while compelling, do not provide conclusive mechanistic evidence. Further studies are required to delineate the upstream signaling pathways, such as AMPK-PGC1α and ROS-mediated pathways.

At the cellular level, our study also found that 2DG treatment shifted the polarization of MxG from a pro-inflammatory to an anti-inflammatory state. In MxG, LPS exposure increased the expression of pro-inflammatory markers such as *Aif1*, *Nos2*, *Tnf*, and *Il6*, while decreasing alternative activation markers like *Il4* and *Il10*. However, 2DG reversed these effects, downregulating pro-inflammatory cytokines and upregulating anti-inflammatory markers such as Arg1. In astrocytes, LPS generates a shift towards an A1 neurotoxic phenotype, characterized by increased expression of markers such as *Lcn2* and *Amigo*, at the expense of the alternative A2 phenotype. However, 2DG reduced A1 markers while promoting A2 markers such as *Clcf4*, *Cd109* and *Ptgs2*,

underscoring its capacity to restore a homeostatic glial state. This shift in polarization is consistent with previous studies showing that metabolic changes in glial cells can influence their inflammatory profiles.

Furthermore, the increase in scavenger gene expression and the enhanced phagocytic activity of 2DG-treated MG point to a shift toward a more regenerative phenotype. For example, 2DG mediated an increase in Galectin-3 and CD206 which are known to play distinct but complementary roles in phagocytosis, and in immune regulation and tissue homeostasis[61,62]. Galectin-3, a β-galactoside-binding lectin, enhances phagocytosis by binding glycosylated surface molecules, promoting receptor clustering, and facilitating actin cytoskeleton remodeling for effective engulfment of apoptotic cells, debris, and pathogens[63]. In contrast, CD206, a mannose receptor predominantly expressed on anti-inflammatory macrophages (M2-like phenotype), specializes in recognizing and internalizing mannose-rich glycoproteins, pathogens, and apoptotic cells[64]. Its role in efferocytosis and non-inflammatory clearance helps maintain tissue homeostasis and promote resolution of inflammation. Together, Galectin-3 and CD206 highlight the dual nature of phagocytosis, balancing immune activation and resolution to adapt to diverse physiological and pathological conditions. This supports the reparative functions of inflammation, emphasizing the therapeutic potential of 2DG for diseases where dysregulated neuroinflammation plays a pivotal role.

Our in vivo studies corroborated these in vitro findings, showing that 2DG treatment in LPS-induced models of neuroinflammation led to reduced levels of pro-inflammatory cytokines such as TNFα and iNOS, while increasing anti-inflammatory markers like *Il4*, *Il10*, and *Arg1*. This suggests that 2DG's ability to modulate glial cell metabolism could have a broad impact on reducing neuroinflammation in the CNS. Notably, 2DG also modulated mitochondrial dynamics and biogenesis markers in vivo, further reinforcing the idea that 2DG acts through multiple cellular pathways to support mitochondrial function and reduce neuroinflammation. Another intriguing finding in our study was the relationship between autophagy and neuroinflammation in the context of 2DG treatment. Autophagy is essential for maintaining cellular homeostasis, particularly under inflammatory conditions. Our data indicate that LPS exposure impaired autophagy-related markers, which were reversed by 2DG treatment. Given that autophagy plays a crucial role in clearing damaged mitochondria and resolving inflammation, these results highlight another mechanism through which 2DG may exert its anti-inflammatory effects. Moreover, our results suggest that 2DG could stimulate mitochondrial biogenesis to compensate for the energy deficits caused by LPS-induced inflammation, ultimately promoting glial cell function and reducing the inflammatory burden.

Our results also showed that a key mediator in the effects of 2DG might be the AMPK pathway, a central regulator of cellular energy homeostasis[65]. Activation of AMPK by 2DG induces a metabolic shift from glycolysis to oxidative phosphorylation, which can profoundly influence glial function. In MG, AMPK activation has been associated with reduced pro-inflammatory cytokine production[66] and enhanced autophagy[67], promoting a phenotype aligned with repair and recovery[66]. Similarly, in MxG, AMPK activation may facilitate adaptive responses to metabolic stress[68], supporting glial survival and function under inflammatory conditions. Our in vivo studies indicated that 2DG could enhance the AMPK activity by phosphorylation of AMPK. This interplay between 2DG and the AMPK pathway may have broader implications for neuroprotection. For instance, pAMPK has been shown to play a critical role in regulating the inflammatory response by modulating the activity of the NF-κB signaling pathway[42]. pAMPK inhibits NF-κB activation through multiple mechanisms, including reducing the degradation of IκBα, an inhibitory protein that sequesters NF-κB in the cytoplasm, thereby preventing its translocation to the nucleus. Interestingly, PGC1α, a master regulator of mitochondrial biogenesis, exerts anti-inflammatory effects by inhibiting NF-κB, as well[69,70]. PGC1α can interact with transcription factors to enhance antioxidant gene expression, reducing ROS levels that otherwise activate NF-κB[70]. Collectively, pAMPK and PGC-1α converge to dampen NF-κB-driven inflammation, promoting cellular homeostasis and repair. By modulating cellular metabolism, 2DG can potentially enhance the resilience of glial cells to oxidative stress, a common feature of neuroinflammatory environments. This mechanism underscores the therapeutic promise of targeting metabolic pathways to regulate glial behavior and mitigate neuroinflammation. In conclusion, as summarized in Fig. S8 (summary Figure) and Fig. S9, our study provides compelling evidence that 2DG modulates metabolic reprogramming, mitochondrial dynamics, and the inflammatory phenotype of MG and astrocytes, offering a potential therapeutic strategy for neuroinflammatory diseases. By shifting glial metabolism back toward OXPHOS and enhancing mitochondrial function, 2DG may not only reduce the neuroinflammatory response but also promote tissue repair and regeneration. However, several limitations need to be considered. The reliance on BV2 cells, MG and MxG may not fully capture the complexity of the broader CNS environment, potentially limiting translational relevance. While we focused on lower doses of 2DG to avoid cytotoxicity, the effects of these doses and their influence on glucose metabolism of other cells necessary for CNS homeostasis remain unexplored. Although many pathways we found to be modulated by 2DG have been implicated in inflammatory and metabolic functions, such as AMPK, NF-κB, and autophagy, our studies do not definitively establish the causal role of these pathways in mediating downstream effects of 2DG in our models. Furthermore, the use of LPS as a neuroinflammation model does not fully replicate disease-specific conditions seen in neurodegenerative disease or trauma. Additionally, the study emphasizes short-term outcomes without addressing long-term effects on repair mechanisms like remyelination or functional recovery. Future studies should address these limitations, including evaluating long-term effects and validating findings in animal models of neurodegenerative diseases, to enhance the translational application of 2DG in managing neuroinflammatory conditions.

Materials and methods

Animals

Pregnant female C57BL/6J mice and seven-week-old male wild-type C57BL/6J mice (strain #: 000664) were purchased from The Jackson Laboratory and acclimated for 7 days. All animal care followed the Guide for the

Care and Use of Laboratory Animals, and experimental protocols were approved by the IACUC (MO24M348) and complied with the ARRIVE guidelines. Mice were housed in a temperature-controlled room (21–25 °C) with 45–65% humidity and a 12-h light/dark cycle, with free access to food and water. They were fed a standard diet low in fiber (5%), protein (20%), and fat (5–10%), and all feed was irradiated or autoclavable. Mice were handled in biosafety cabinets using aseptic techniques, protective clothing, high-level disinfectants (MB-10), and procedures to prevent cross-contamination between cages. Mice were euthanized by high-concentration isoflurane exposure or, in some cases, by overdose of ketamine/xylazine, in accordance with IACUC guidelines.

Cell culture

Primary cell cultures

Mixed glial culture Mixed glial cells (MxG) were prepared from P0-P2 C57BL/6 mouse pups of both sexes, as we previously reported[39,71]. Briefly, brains were isolated and while maintained in cold DMEM/F12 (cat. No. 11330, Invitrogen, Carlsbad, CA, USA), cortices were separated, and meninges were stripped under a dissection microscope. Cortices were placed in a 15 mL centrifuge tube and a serological pipet was used to remove the excess buffer before adding 1 mL of 0.05% Trypsin (Gibco Cat #25300) per brain. Before incubating the cortices for 15 min at 37 °C in an incubator, they were dissociated in trypsin with a 10 mL serological pipet. After 15 min, trypsin was neutralized with an equal volume of DMEM/F12 containing 1% penicillin-streptomycin and 10% FBS. Brains were then homogenized with 6 mL DMEM/F12 with a 5 mL serological pipet fixed to a 1 mL sterile pipet tip by pipetting several times. The cell suspension was filtered twice through a 100 µm cell strainer into a 50 mL conical tube and centrifuged at 1000 rpm for 10 min. The cell suspension was seeded into poly-D-lysine-coated (PDL; Sigma-Aldrich, cat # 27964-99-4) T150 tissue culture flasks pre-coated with 100 mg/mL PDL at 37 °C overnight. Media was replaced every three days and maintained in DMEM/F12 with 10% FBS and 1% penicillin-streptomycin for 10–14 days to grow a confluent MxG containing astrocytes and microglia. Upon confluency (80–90%), they were sub-cultured with trypsin 0.05% for further experiments.

Microglia culture We obtained our microglia (MG) with two different methods. For the Seahorse and JC-1 assay, we enriched MG from MxG using a shaker. MxG were cultured in a 175 cm^2 culture flask for two weeks. Flasks were then stacked on a flat platform shaker and shaken at 180 rpm for 30 min. After shaking, the media was collected in a 50 mL conical tube and centrifuged at 500 x g for 6 min at 4 °C. The cell pellet was resuspended in DMEM/F12 containing 1% penicillin-streptomycin and 10% FBS. After determining the cell number, we seeded 2×10^4 enriched MG per well in a 96-well plate. For mitochondrial fragmentation studies using Mito Tracker, immunocytochemical (ICC) staining, as well as phagocytosis assay, MG were isolated from 4-week-old C57BL/6J mice of both sexes following a previously described protocol[39]. Briefly, cortices were finely minced in cold enzyme digestion buffer containing HBSS (without calcium/magnesium), 5% FBS, 10 µM HEPES, 2 mg/mL collagenase D, and 28 U/mL DNase I. The tissue was triturated to obtain a single-cell suspension, filtered through a 70-µm filter, and centrifuged at 300 g for 10 min at 4 °C. Debris was removed, and cells were incubated with CD11b magnetic microbeads (Miltenyi Biotec) for 15 min on ice with gentle mixing every 5 min. $CD11b^+$ cells were isolated using a MACS LS column (Miltenyi Biotec), centrifuged, and resuspended in DMEM/F12 supplemented with 1% penicillin-streptomycin, 2 mM glutamine, 5 µg/mL *N*-acetyl-L-cysteine, 1x SATO, 10% FBS, and 20 ng/mL M-CSF. Microglia were cultured in a PDL-coated plate for 7 days in vitro before being used in assays. The purity of MG was evaluated by immunocytochemical (ICC) staining using antibodies against ionized calcium binding adapter molecule 1 (iba1; 1:1000; Wako Pure Chemical Industries, Ltd., Richmond, VA) and 40,6-diamidino- 2-phenylindole (DAPI) (1:1000; Sigma–Aldrich) and was routinely greater than 90%, while glial fibrillary acidic protein (GFAP) (1:3000; Sigma–Aldrich) staining was negligible (data not shown).

BV2 microglial cell culture

BV2 cells were cultured in DMEM (Dulbecco's Modified Eagle Medium) supplemented with 10% fetal bovine serum (FBS), 1% penicillin-streptomycin, and 2 mM glutamine. The cells were maintained at 37 °C in a humidified incubator with 5% CO_2. BV2 cells were sub-cultured once they reached approximately 70–80% confluency. For experiments, cells were seeded at a density of 2×10^4 cells per well in a 96-well plate or 30×10^4 cells per well in a 6-well plate, depending on the assay requirements. Media was replaced every 2–3 days to ensure optimal cell growth and viability throughout the experiment.

Drugs and reagents

Lipopolysaccharide (LPS, #L6529 from Escherichia coli, O55:B5) and 2-Deoxy-D-Glucose (2DG, D8375) were both purchased from Sigma-Aldrich (St. Louis, MO, USA) and diluted in sterile endotoxin free water as a stock solution to be used for in vitro and in vivo studies. They were further diluted in saline as a working solution for in vivo studies. Mito Stress test kit containing Oligomycin (Olig), Carbonyl cyanide 4-trifluoromethoxy-phenylhydrazone (FCCP), Rotenone (R), and Antimycin A (A) purchased from Agilent (103015-100, Agilent Technologies) and used following the manufacturer's instructions for preparation and dilution. 5,5′,6,6′-tetrachloro1,1′,3,3′-tetramethylbenzimidazolylcarbocyanine iodide (JC-1) dye was purchased from Invitrogen (#65-0851-38). Mito Tracker® Red CMXRos was obtained from Cell Signaling (9082). Sapphire-700 for cell viability assay was obtained from LI-COR (928-40022) and we used SYBR Green PowerUP from Applied Biosystems (A25741) for performing reverse transcriptase quantitative real-time Polymerase Chain Reaction (RT-qPCR).

Measurement of oxygen consumption rate

Real-time measurements of oxygen consumption rates (OCR) from mitochondrial respiration were executed on an XFe96 Seahorse extracellular flux analyzer (Agilent Technologies). Briefly, 2×10^4 cells per well in a Seahorse PDL-coated 96-well plate (Agilent) were seeded 3 days before the experiment and incubated at 37 °C. Before

performing the Seahorse assay, the medium was removed and replaced with assay medium containing XF Base medium minimal DMEM (Agilent) complemented with 2 mM glucose, 2 mM glutamax, and 1mM pyruvate. The cells were incubated for 30 min in a 37 °C non-CO^2 incubator immediately prior to the assay. Mito Stress assay was then performed using Seahorse XF Cell Mito Stress Test Kit (103015-100, Agilent Technologies) strictly following the manufacturer's protocol (Mito_Stress_Test_Kit_Guide). With this system, OCR was measured at baseline (basal respiration or BR) before drug injection and then quantified in real-time after sequential addition of 2 mM Oligo, 1 mM FCCP, and 5 mM R and A (RA). Spare respiratory capacity (SC) was calculated by subtracting the OCR of BR from the maximal OCR induced by FCCP. All data presented as BR and SC in Figs. 1, 2 and 3 are shown as fold change, as they were normalized to untreated cells.

Measurement of OCR in isolated mitochondria: OCR was additionally measured in isolated mitochondria from whole mouse brain homogenates to study LPS- and 2-DG-related changes in mitochondrial OCR in an in vivo system. Mice were euthanized, and brains were extracted and homogenized using a mitochondrial isolation buffer (MIB; pH 7.2–7.4) containing 75 mM sucrose, 215 mM mannitol, 0.1% BSA, 20 mM HEPES, and 1 mM EGTA. Cellular debris and myelin were removed via two centrifugation steps (1300 g, 3 min) followed by filtration through a cheesecloth[72]. This solution of isolated mitochondria was centrifuged at high speed (13,000 g, 10 min), and the pellet was resuspended in a KCl-based medium compatible with the Seahorse assay, containing 125 mM KCl, 2 mM $MgCl_2$, 2.5 mM KH_2PO_4, 20 mM HEPES, and 0.1% BSA (pH 7.2–7.4). BCA was used to determine sample protein concentration, and 10 µg of protein was loaded per well in Seahorse assay plates. The Seahorse assay was performed as indicated above by the manufacturer's protocol.

Measurement of mitochondrial membrane potential

The JC-1 dye was used to monitor mitochondrial membrane potential (MMP). The monomeric form has an emission maximum of ~ 529 nm. The dye at higher concentrations or potentials forms red fluorescent aggregation with an emission maximum of ~ 590 nm. The ratio of this green/red fluorescence is independent of mitochondrial shape, density, or size, but depends only on membrane potential. In healthy mitochondria with high membrane potential, JC-1 forms an aggregate that emits red fluorescence, whereas in depolarized mitochondria with reduced MMP, it remains in its monomeric form, emitting green fluorescence. A decreased red/green fluorescence ratio reflects mitochondrial depolarization and dysfunction. For this study, MxG and MG were grown on PDL-coated 96-well plates prior to JC-1 staining. MxG and MG were stimulated with LPS (200 ng/mL) for 24 h, then the media were replaced with fresh media containing vehicle or 2DG (200 µM) for an additional 24 h. According to the manufacturer's protocol, we prepared a fresh 200 µM JC-1 dye stock solution immediately before use by reconstructing the lyophilized JC-1 dye with DMSO to obtain a 100× stock solution. The cell culture medium was aspirated, and 100 µl of media containing 2µM JC-1 was applied to the cells. Following incubation at 37 °C for 10 min in a light-proof cell incubator, the media was aspirated, and the cells were rinsed 3 times using media with no JC-1. Then the cells were immediately scanned using a confocal microscope in Hanks' balanced salt solution (HBSS) with Ca2 + and Mg2 + but no phenol red (Invitrogen 14025-092). FITC and PE fluorescence readings were used to measure MMP, while FITC fluorescence was detected at 488 nm and 530 nm and the PE fluorescence signal was excited at 530 nm and detected at 630 nm. Acquired images were processed using ImageJ to measure the fluorescence intensity.

Measurement of complex-V activity

Complex-V/ATP synthase is the terminal enzyme of the mitochondrial electron transport chain responsible for ATP synthesis, and thus complex-V activity is a useful quantitative indicator of mitochondrial oxidative phosphorylation. For this purpose, the Mitochondrial Complex-V Activity Assay Kit (NBP3-25842, Novus Biologicals) was employed to measure complex-V activity from whole mouse brain tissue, homogenized in MIB. This colorimetric assay operates on the principle that complex-V mediates a reversible reaction between ATP synthesis and hydrolysis: ATP hydrolysis to ADP allows ADP-mediated conversion of NADH to NAD^+ after the enzyme conversion reaction. Complex-V activity is quantified using the change in absorption at 340 nm. The manufacturer's protocol was closely followed for tissue preparation, mitochondrial isolation, and complex-V activity measurement.

Measurement of reactive oxygen species generation

Inflammatory processes are known to stimulate the generation of reactive oxygen species (ROS), which further propagate inflammation and free radical-mediated cellular injury. To determine whether 2DG may mitigate LPS-induced ROS generation in vivo, we utilized the OxiSelect™ In Vitro ROS/RNS Assay Kit (STA-347, Cell Biolabs) to quantify ROS generation in whole mouse brain tissue, homogenized in MIB. This fluorescence assay uses a quenched fluorogenic probe that reacts with ROS in samples, resulting in oxidation of the probe into a fluorescent form. Fluorescence was measured using a fluorescence plate reader at 485 nm excitation/530 nm emission. The manufacturer's protocol was closely followed for tissue preparation and ROS quantification.

Measurement of mitochondrial fragmentation

MG isolated with $CD11b^+$ magnetic beads were cultured on PDL-coated coverslips 7 days before performing the experiment. The cells were incubated with MG media containing LPS (200 ng/mL) for 24 h, then switched to fresh MG media containing vehicle or 2DG (200 µM) for an additional 24 h. To track mitochondrial morphology, cells were incubated in an MG media containing 100 nM Mito Tracker for 30 min following the user's manual for preparation and dilution. After incubation, cells were fixed in ice-cold methanol for 15 min at – 20 °C and then rinsed 3 times with PBS for 5 min. Following DAPI staining, coverslips were mounted on the slides for confocal imaging using a 96× oil immersion lens. Acquired images were processed using the open-source ImageJ/Fiji -> Mitochondria analyzer plugin to assess the two-dimensional (2D) analysis of mitochondrial morphology and

network connectivity. For 2D analysis, using the Chaudhry et al. method[33] we characterized mitochondrial size by area and perimeter, whereas mitochondrial shape was defined by form factor (FF) and aspect ratio (AR). We evaluated the mitochondrial network's overall connectivity and morphological complexity based on the skeletonized network. We quantified this by the number of branches and branch junctions, as well as the length of branches in the skeleton. Supplemental Fig. S3 summarizes the mitochondrial labeling and indicates how they change with various morphologies.

In vivo LPS models of neuroinflammation

LPS induces activation of MG into a pro-inflammatory state and astrocytes into a reactive state, both mediated via toll-like receptor 4 (TLR4), contributing to neuroinflammation. LPS administration is commonly used to model neuroinflammation in mice that is accompanied by metabolic reprogramming in both cell types. In this study, neuroinflammation was induced by intraperitoneal (ip) or intracerebroventricular (icv) injections of LPS to explore metabolic changes, and the potential modulatory effects of 2DG (ip) were assessed. Mice were divided into treatment groups for ip injection as follows: (I) ip saline: no treatment (NT), (II) ip LPS (500 µg/kg) plus vehicle (saline): LPS group, and (III) ip LPS (500 µg/kg) with 2DG (100 mg/kg): LPS + 2DG group. For icv injection, the groups were (IV) icv saline: sham, (V) icv LPS (12 µg in 3 µl) with ip saline: LPS icv group, and (VI) icv LPS (12 µg in 3 µl) with ip 2DG (100 mg/kg): LPS icv 2DG ip group. Each group included five male mice. Intraperitoneal LPS was administered daily for seven consecutive days, with saline as the control. The icv injection was performed bilaterally using stereotactic surgery (ketamine;100 mg/kg and xylazine;10 mg/kg) at the coordinates 0.5 mm posterior and ± 1.5 mm lateral to the bregma, with 3 µl of saline or LPS (12 µg) delivered into each lateral ventricle at a depth of 2.6 mm (at the rate of 1 µl/min). After injection, the needle remained in place for 2 min to prevent backflow. For both ip and icv LPS treatment paradigms, mice received 2DG or saline (ip) daily for seven days and were euthanized on day 7, with brains harvested for qPCR and WB analysis. The left cerebrum was used for qPCR, and the right cerebrum was used for immunoblotting. In one cohort (treatment groups I, II, and III; $n = 5$), whole brains were collected, homogenized in MIB, and used for Seahorse analysis, complex-V activity measurement, and ROS assays. Mitochondria were further purified for use in the Seahorse assay as indicated in "Measurement of oxygen consumption rate".

RT-qPCR

Total RNA from MxG or mouse brain (following in vivo LPS treatment) was extracted using RNeasy kit (QIAGEN), and reverse transcribed into cDNA with High-Capacity RNA-to-cDNA™ Kit (Applied Biosystems). RT-qPCR was performed in triplicate for each sample using PowerUp SYBR Green Master Mix (Applied Biosystems) with a CFX384 Real-Time System (Bio-Rad). For each reaction, 10 ng of cDNA was used. Primers are listed in Table S1. Relative expression values were calculated using the $2^{-\Delta\Delta CT}$ method and normalized against peptidylprolyl isomerase-A (ppia) or β-2-microglobulin (B2m) for MxG and brain samples.

Western immunoblotting (WB)

Mouse brains were homogenized and lysed on ice in RIPA buffer supplemented with protease and phosphatase inhibitors. The protein concentration was determined by BCA assay, and samples were prepared in NuPAGE LDS Sample Buffer (Invitrogen). The samples were then run on a NuPAGE 4–12% Bis-Tris gel (Thermo Fisher Scientific) and transferred to a PVDF Immobilon-P membrane (Millipore). The membrane was blocked in Intercept© Blocking buffer (LI-COR, 927-60001) for 1 h at room temperature (RT) and incubated overnight at 4 °C with antibodies against primary antibodies listed in Table S2. This was followed by incubation with IRDye 800CW and 680RD anti-rabbit, -mouse or -goat secondary antibodies (1:15,000) for 2 h at RT. The blot was visualized with the LI-COR imaging system. GAPDH or β-tubulin was used to verify sample loading. The blot quantification was performed using ImageJ software. In some cases, lanes were spliced together in the main figures in order to show different conditions next to one another while conserving space; however, any adjustments were applied to the entire blot equally before splicing. Full scans of key Western blot data are shown in Fig. S7.

InCell western immunoblotting (InCell WB)

To perform an InCell Western blot, we used the LI-COR Odyssey system. MxG (3×10^4 cells per well) were seeded in a pre-coated PDL 96-well plate 24 h before beginning the experiments. After completing experiments, the culture media were removed, and the cells were washed with PBS. Cells were then fixed by adding 4% paraformaldehyde (PFA) and incubating at 4 °C for 15 min, followed by 2–3 PBS washes. To permeabilize the cells, 0.1% Triton X-100 in PBS was added and incubated for 10 min. The permeabilization buffer was removed with additional PBS washes. To block non-specific binding, cells were incubated with LI-COR Odyssey blocking buffer for 1 h at room temperature. Primary antibodies (listed in Table S2) were diluted in blocking buffer and added to the wells, with overnight incubation at 4 °C. β-tubulin was used as a housekeeping protein. After incubation, cells were washed 3 times with PBS containing 0.1% Tween-20 for 5 min per wash. IRDye-conjugated secondary antibodies (listed in Table S2) diluted in blocking buffer were then added and incubated for 1 h at room temperature in the dark. The cells were washed again with PBS containing 0.1% Tween-20, protecting them from light to maintain fluorescence. The plate was scanned using the LI-COR Odyssey Imaging System, and data were analyzed for fluorescence intensity using ImageJ. Appropriate controls, including the absence of primary antibodies, were used to account for background fluorescence.

Viability assay

Sapphire-700 is a non-permeable dye that does not fluoresce when added to intact cells but becomes fluorescent upon binding to intracellular proteins when the cell membrane is compromised. This fluorescence can be

detected using near-infrared imaging in the 700 nm channel with the LI-COR system and is directly proportional to the number of dead cells with damaged membranes. The assay measures total fluorescence in each well but does not quantify individual cells. For this assay, MxG (3×10^4 cells per well) were seeded into pre-coated PDL 96-well plates 24 h before treatment. After the experimental treatments, the media was removed, and the cells were washed with PBS. DMEM containing Sapphire-700 (1:50 v/v) was then added to each well, and the plate was incubated at 37 °C in a humidified CO2 incubator for 30 min. The plate was scanned using the LI-COR Odyssey system with detection in the 700 nm channel. After scanning, the cells were washed three times with PBS and fixed with 4% PFA for 10 min at 4 °C. To normalize the data, the cells were stained with β-tubulin as a housekeeping protein, and the intensity of each well was normalized to the untreated group.

Immunocytochemistry

$CD11b^+$ MG were plated on PDL-coated glass coverslips in a 24-well cell culture plate in DMEM/F12 supplemented with 1% penicillin-streptomycin, 2 mM glutamine, 5 µg/mL *N*-acetyl-L-cysteine, 1x SATO, 10% FBS, and 20 ng/mL M-CSF for 7 days prior to beginning the experiments. Following experimental treatments, MG was washed three times with PBS and fixed with 4% PFA for 10 min at 4 °C. The cells were then washed twice in TBS and permeabilized with 1% Triton X-100 in TBS (TBS-T) for 5 min, followed by incubation in blocking solution (5% donkey serum, 5% goat serum in TBS) for 45 min at RT. The cells were then incubated with primary antibodies (listed in Table S2) diluted in (20% blocking buffer in TBS) overnight at 4 °C. The cells were then washed three times with the TBS buffer for 5 min. Appropriate Alexa Fluor conjugated secondary antibodies (listed in Table S2) in 20% blocking buffer in TBS were added for 2 h at RT and then stained with DAPI. Images were taken on Zeiss LSM 700 Confocal. Double-positive cells were counted in a blinded fashion.

Myelin isolation, labeling, and phagocytosis assay

Myelin isolation and labeling

Myelin was isolated and labeled with carboxyfluorescein succinimidyl ester (CFSE, Thermo Fisher Scientific) as previously described[39] to obtain fluorescent-tagged myelin particles (FTMP). Briefly, brains from ten 8–10-week-old C57BL/6J mice were dissected and placed in ice-cold 0.32 M sucrose solution. The brains were cut into small pieces (~ 5 mm^2) and transferred to 30 mL of the same solution. The tissue was homogenized using a sterile hand-held rotary homogenizer. The brain homogenate was layered on top of ice-cold 0.83 M sucrose in a 50-mL centrifuge tube and centrifuged at 100,000 g for 45 min at 4 °C in an ultracentrifuge. The myelin debris, seen as a white band at the interface between the two sucrose layers, was collected, re-homogenized, and centrifuged again at 100,000 g for 45 min. The resulting myelin pellet was resuspended in Tris-Cl buffer (pH 7.4) and centrifuged again. The pellet was then suspended in sterile PBS and centrifuged at 22,000 g for 10 min at 4 °C. The final myelin pellet (100 mg/mL) was resuspended in PBS. For myelin labeling, 100 µl of the isolated myelin was resuspended in 200 µl of 50 µM CFSE, incubated for 30 min at room temperature in the dark, and centrifuged at 14,800 g for 10 min at 4 °C. Labeled myelin was washed three times with 100 mM glycine in PBS and resuspended in sterile PBS (final concentration 100 mg/mL).

Phagocytosis assay

$CD11b^+$ MG were cultured in pre-coated PDL 96-well plates at 2×10^4 cells per well. Cells were treated for 24 h with LPS (200 ng/mL) or vehicle, then the media was replaced with fresh media containing 2DG (200 µM) or vehicle for an additional 24 h. The cells were washed 2x with PBS and incubated with CFSE-labeled myelin (FTMP) (1 mg/mL) for 2 h at 37 °C and washed three times with PBS to remove non-engulfed myelin. MG were fixed with 4% PFA, blocked in 10% mouse serum, and incubated overnight at 4 °C with β-tubulin antibody, followed by washing and incubation with a secondary antibody conjugated with IRDye 680RD for 1 h at RT. The images were scanned with the LI-COR Odyssey system, and each well's fluorescence intensity was calculated using ImageJ software and normalized first to the housekeeping protein β-tubulin and then to the vehicle group.

Data availability

All data supporting the findings of this study are presented and/or tabulated within the article or supplementary figures. The datasets generated and analyzed during the current study are available from the corresponding author upon reasonable request.

Received: 8 February 2025; Accepted: 30 September 2025
Published online: 06 November 2025

References

1. Adamu, A., Li, S., Gao, F. & Xue, G. The role of neuroinflammation in neurodegenerative diseases: current Understanding and future therapeutic targets. *Front. Aging Neurosci.* **16**, (2024).
2. Schimmel, S. J., Acosta, S. & Lozano, D. Neuroinflammation in traumatic brain injury: A chronic response to an acute injury. *Brain Circ.* **3**, 135–142 (2017).
3. Stephenson, J., Nutma, E., van der Valk, P. & Amor, S. Inflammation in CNS neurodegenerative diseases. *Immunology* **154**, 204 (2018).
4. Fisher, T. M. & Liddelow, S. A. Emerging roles of astrocytes as immune effectors in the central nervous system. *Trends Immunol.* **45**, 824–836 (2024).
5. Linnerbauer, M., Wheeler, M. A. & Quintana, F. J. Astrocyte crosstalk in CNS inflammation. *Neuron* **108**, 608 (2020).
6. Rauf, A. et al. Neuroinflammatory markers: key indicators in the pathology of neurodegenerative diseases. *Molecules* **27**, 3194 (2022).
7. Sangineto, M. et al. Metabolic reprogramming in inflammatory microglia indicates a potential way of targeting inflammation in alzheimer's disease. *Redox Biol.* **66**, 102846 (2023).

8. Huang, Q., Wang, Y., Chen, S. & Liang, F. Glycometabolic reprogramming of microglia in neurodegenerative diseases: insights from neuroinflammation. *Aging Dis.* **15**, 1155–1175 (2024).
9. Afridi, R., Rahman, M. H. & Suk, K. Implications of glial metabolic dysregulation in the pathophysiology of neurodegenerative diseases. *Neurobiol. Dis.* **174**, 105874 (2022).
10. Wang, H. et al. Target modulation of glycolytic pathways as a new strategy for the treatment of neuroinflammatory diseases. *Ageing Res. Rev.* **101**, 102472 (2024).
11. Patergnani, S., Bouhamida, E., Leo, S., Pinton, P. & Rimessi, A. Mitochondrial oxidative stress and mito-inflammation: actors in the diseases. *Biomedicines* **9**, 216 (2021).
12. Pajak, B. et al. 2-Deoxy-d-Glucose and its analogs: from diagnostic to therapeutic agents. *Int. J. Mol. Sci.* **21**, 234 (2019).
13. Wick, A. N., Drury, D. R., Nakada, H. I. & Wolfe, J. B. Localization of the primary metabolic block produced by 2-deoxyglucose. *J. Biol. Chem.* **224**, 963–969 (1957).
14. Hellemann, E. et al. Novel mutation in hexokinase 2 confers resistance to 2-deoxyglucose by altering protein dynamics. *PLoS Comput. Biol.* **18**, e1009929 (2022).
15. Pålsson-McDermott, E. M. & O'Neill, L. A. J. Targeting immunometabolism as an anti-inflammatory strategy. *Cell. Res.* **30**, 300–314 (2020).
16. Ahadova, A., Gebert, J., von Knebel Doeberitz, M., Kopitz, J. & Kloor, M. Dose-dependent effect of 2-deoxy-D-glucose on glycoprotein mannosylation in cancer cells. *IUBMB Life*. **67**, 218–226 (2015).
17. Lee, C. F. et al. Preventing allograft rejection by targeting immune metabolism. *Cell. Rep.* **13**, 760 (2015).
18. Yin, Y. et al. Normalization of CD4 + T cell metabolism reverses lupus. *Sci. Transl. Med.* **7**, 274ra18 (2015).
19. Francis, R., Singh, P. K., Singh, S., Giri, S. & Kumar, A. Glycolytic inhibitor 2-deoxyglucose suppresses inflammatory response in innate immune cells and experimental Staphylococcal endophthalmitis. *Exp. Eye Res.* **197**, 108079 (2020).
20. Shen, Y. et al. Bioenergetic state regulates innate inflammatory responses through the transcriptional co-repressor CtBP. *Nat. Commun.* **8**, 624 (2017).
21. Vilalta, A. & Brown, G. C. Deoxyglucose prevents neurodegeneration in culture by eliminating microglia. *J. Neuroinflamm.* **11**, 58 (2014).
22. Bernier, L. P., York, E. M. & MacVicar, B. A. Immunometabolism in the brain: how metabolism shapes microglial function. *Trends Neurosci.* **43**, 854–869 (2020).
23. Lively, S. & Schlichter, L. C. Microglia responses to Pro-inflammatory stimuli (LPS, IFNγ + TNFα) and reprogramming by resolving cytokines (IL-4, IL-10). *Front. Cell. Neurosci.* **12**, 215 (2018).
24. Zamanian, J. L. et al. Genomic analysis of reactive astrogliosis. *J. Neurosci.* **32**, 6391–6410 (2012).
25. Yates, D. A toxic reaction. *Nat. Rev. Neurosci.* **18**, 130–130 (2017).
26. Li, K., Li, J., Zheng, J. & Qin, S. Reactive astrocytes in neurodegenerative diseases. *Aging Dis.* **10**, 664–675 (2019).
27. Brown, G. C. The endotoxin hypothesis of neurodegeneration. *J. Neuroinflamm.* **16**, 180 (2019).
28. Gao, C., Jiang, J., Tan, Y. & Chen, S. Microglia in neurodegenerative diseases: mechanism and potential therapeutic targets. *Sig Transduct. Target. Ther.* **8**, 359 (2023).
29. Chen, W., Zhao, H. & Li, Y. Mitochondrial dynamics in health and disease: mechanisms and potential targets. *Sig Transduct. Target. Ther.* **8**, 333 (2023).
30. Motori, E. et al. Inflammation-Induced alteration of astrocyte mitochondrial dynamics requires autophagy for mitochondrial network maintenance. *Cell Metabol.* **18**, 844–859 (2013).
31. Charrasse, S. et al. Quantitative imaging and semiotic phenotyping of mitochondrial network morphology in live human cells. *PLoS One*. **19**, e0301372 (2024).
32. Glancy, B., Kim, Y., Katti, P. & Willingham, T. B. The functional impact of mitochondrial structure across subcellular scales. *Front. Physiol.* **11**, 541040 (2020).
33. Chaudhry, A., Shi, R. & Luciani, D. S. A pipeline for multidimensional confocal analysis of mitochondrial morphology, function, and dynamics in pancreatic β-cells. *Am. J. Physiol.-Endocrinol. Metab.* **318**, E87–E101 (2020).
34. Skrzypczak-Wiercioch, A. & Sałat, K. Lipopolysaccharide-induced model of neuroinflammation: mechanisms of action, research application and future directions for its use. *Molecules* **27**, 5481 (2022).
35. da Silva, A. A. F. et al. Lipopolysaccharide-induced animal models for neuroinflammation—An overview. *J. Neuroimmunol.* **387**, 578273 (2024).
36. Batista, C. R. A., Gomes, G. F., Candelario-Jalil, E., Fiebich, B. L. & de Oliveira, A. C. P. Lipopolysaccharide-induced neuroinflammation as a bridge to understand neurodegeneration. *Int. J. Mol. Sci.* **20**, 2293 (2019).
37. Marrocco, A. & Ortiz, L. A. Role of metabolic reprogramming in pro-inflammatory cytokine secretion from LPS or silica-activated macrophages. *Front. Immunol.* **13**, 936167 (2022).
38. Lawrence, J. M., Schardien, K., Wigdahl, B. & Nonnemacher, M. R. Roles of neuropathology-associated reactive astrocytes: a systematic review. *Acta Neuropathol. Commun.* **11**, 42 (2023).
39. Gharibani, P. et al. The protein kinase C modulator bryostatin-1 therapeutically targets microglia to attenuate neuroinflammation and promote remyelination. *Sci. Transl. Med.* **17**, eadk3434 (2025).
40. Zhao, J. et al. Low-dose 2-deoxyglucose and Metformin synergically inhibit proliferation of human polycystic kidney cells by modulating glucose metabolism. *Cell. Death Discov.* **5**, 76 (2019).
41. Rius-Pérez, S., Torres-Cuevas, I., Millán, I., Ortega, Á. L. & Pérez, S. PGC-1α, Inflammation, and Oxidative Stress: An Integrative View in Metabolism. *Oxid. Med. Cell Longev.* **2020**, 1452696 (2020).
42. Salminen, A., Hyttinen, J. M. T. & Kaarniranta, K. AMP-activated protein kinase inhibits NF-κB signaling and inflammation: impact on healthspan and lifespan. *J. Mol. Med. (Berl).* **89**, 667–676 (2011).
43. Zong, Y. et al. Mitochondrial dysfunction: mechanisms and advances in therapy. *Sig Transduct. Target. Ther.* **9**, 124 (2024).
44. Kwon, H. S. & Koh, S. H. Neuroinflammation in neurodegenerative disorders: the roles of microglia and astrocytes. *Transl. Neurodegener.* **9**, 42 (2020).
45. Müller, L., Di Benedetto, S. & Müller, V. From homeostasis to neuroinflammation: insights into cellular and molecular interactions and network dynamics. *Cells*. **14**, 54 (2025).
46. Laussel, C. & Léon, S. Cellular toxicity of the metabolic inhibitor 2-deoxyglucose and associated resistance mechanisms. *Biochem. Pharmacol.* **182**, 114213 (2020).
47. Chiaravalli, M. et al. 2-Deoxy-d-Glucose ameliorates PKD progression. *J. Am. Soc. Nephrol.* **27**, 1958–1969 (2016).
48. Koenig, J. B. et al. Glycolytic inhibitor 2-deoxyglucose prevents cortical hyperexcitability after traumatic brain injury. *JCI Insight* **4**, e126506.
49. Aiestaran-Zelaia, I. et al. 2 deoxy-D-glucose augments the mitochondrial respiratory chain in heart. *Sci. Rep.* **12**, 6890 (2022).
50. Mukherjee, A. & Haldar, C. Effect of 2-deoxy-d-glucose induced metabolic stress on testicular steroidogenesis and antioxidant status in golden hamster,*Mesocricetus auratus*: role of photoperiod. *J. Photochem. Photobiol. B.* **153**, 40–50 (2015).
51. Zheng, J. et al. GLP-1 improves the supportive ability of astrocytes to neurons by promoting aerobic Glycolysis in alzheimer's disease. *Mol. Metab.* **47**, 101180 (2021).
52. Ibork, H. et al. Cannabidiol-rich *Cannabis sativa* L. extract alleviates LPS-induced neuroinflammation behavioral alterations, and astrocytic bioenergetic impairment in male mice. *J. Neurosci. Res.* **103**, e70035 (2025).
53. Ivanov, A. I. et al. Glycolysis and oxidative phosphorylation in neurons and astrocytes during network activity in hippocampal slices. *J. Cereb. Blood Flow. Metab.* **34**, 397–407 (2014).

54. Dias, C., Fernandes, E., Barbosa, R. M., Laranjinha, J. & Ledo, A. Astrocytic aerobic glycolysis provides lactate to support neuronal oxidative metabolism in the hippocampus. *BioFactors* **49**, 875–886 (2023).
55. Hansen, M. E. et al. Lipopolysaccharide disrupts mitochondrial physiology in skeletal muscle via disparate effects on sphingolipid metabolism. *Shock* **44**, 585–592 (2015).
56. Esteves, A. R. et al. LPS-induced mitochondrial dysfunction regulates innate immunity activation and α-synuclein oligomerization in parkinson's disease. *Redox Biol.* **63**, 102714 (2023).
57. Kuznetsov, A. V. et al. Structural and functional remodeling of mitochondria as an adaptive response to energy deprivation. *Biochim. Et Biophys. Acta (BBA) - Bioenergetics.* **1862**, 148393 (2021).
58. Palikaras, K., Lionaki, E. & Tavernarakis, N. Balancing mitochondrial biogenesis and mitophagy to maintain energy metabolism homeostasis. *Cell. Death Differ.* **22**, 1399–1401 (2015).
59. Gao, W. et al. Dissecting the crosstalk between Nrf2 and NF-κB response pathways in Drug-Induced toxicity. *Front. Cell. Dev. Biol.* **9**, 809952 (2021).
60. Vomund, S., Schäfer, A., Parnham, M. J., Brüne, B. & von Knethen, A. Nrf2, the master regulator of anti-oxidative responses. *Int. J. Mol. Sci.* **18**, 2772 (2017).
61. Díaz-Alvarez, L. & Ortega, E. The many roles of galectin-3, a multifaceted molecule, in innate immune responses against pathogens. *Mediat. Inflamm.* **2017**, 9247574 (2017).
62. Azad, A. K., Rajaram, M. V. S. & Schlesinger, L. S. Exploitation of the macrophage mannose receptor (CD206) in infectious disease diagnostics and therapeutics. *J. Cytol. Mol. Biol.* **1**, 1000003 (2014).
63. Rotshenker, S. Galectin-3 (MAC-2) controls phagocytosis and macropinocytosis through intracellular and extracellular mechanisms. *Front. Cell. Neurosci.* **16**, 949079 (2022).
64. Jaynes, J. M. et al. Mannose receptor (CD206) activation in tumor-associated macrophages enhances adaptive and innate antitumor immune responses. *Sci. Transl. Med.* **12**, eaax6337 (2020).
65. Long, Y. C. & Zierath, J. R. AMP-activated protein kinase signaling in metabolic regulation. *J. Clin. Investig.* **116**, 1776–1783 (2006).
66. Noor, H. B. et al. Anti-inflammatory property of AMP-activated protein kinase. *Antiinfect Agents Med. Chem.* **19**, 2–41 (2020).
67. Zhang, C. S. & Lin, S. C. AMPK promotes autophagy by facilitating mitochondrial fission. *Cell Metabol.* **23**, 399–401 (2016).
68. Craig, P. M., Moyes, C. D. & LeMoine, C. M. R. Sensing and responding to energetic stress: evolution of the AMPK network. *Comp. Biochem. Physiol. B Biochem. Mol. Biol.* **224**, 156–169 (2018).
69. Austin, S. & St-Pierre, J. PGC1α and mitochondrial metabolism–emerging concepts and relevance in ageing and neurodegenerative disorders. *J. Cell. Sci.* **125**, 4963–4971 (2012).
70. Abu Shelbayeh, O., Arroum, T., Morris, S. & Busch, K. B. PGC-1α is a master regulator of mitochondrial lifecycle and ROS stress response. *Antioxid. (Basel).* **12**, 1075 (2023).
71. Abramson, E. et al. Designed PKC-targeting Bryostatin analogs modulate innate immunity and neuroinflammation. *Cell. Chem. Biol.* **28**, 537–545e4 (2021).
72. Acín-Pérez, R. et al. Isolation of mitochondria from mouse tissues for functional analysis. *Methods Mol. Biol.* **2675**, 77–96 (2023).

Acknowledgements
We would like to thank Peter Calabresi and Ahmet Hoke for providing access to equipment used for our study and Yasmin Resto for her administrative and lab management support.

Author contributions
P.G. and M.D.K. conceptualized the study. P.G. and M.D.K. curated the data. P.G., Y.G., S.S., P.M.K., and M.D.K. performed data analysis. M.D.K. acquired funding. P.G., Y.G., S.S., J.J.L. and K.K. performed experiments. M.D.K. performed project administration. P.M.K. and M.D.K. provided resources. P.G. and M.D.K. supervised the study. P.G., Y.G., S.S., K.K., P.M.K., and M.D.K. visualized the data. P.G. and M.D.K. wrote the original draft of the manuscript. P.G., Y.G., S.S., J.J.L., K.K., P.M.K., and M.D.K. reviewed and edited the manuscript.

Funding
This work was supported by the National Institutes of Health grant K08NS104266 (to MDK).

Declarations

Competing interests
The authors declare no competing interests.

Additional information
Supplementary Information The online version contains supplementary material available at https://doi.org/10.1038/s41598-025-22677-w.

Correspondence and requests for materials should be addressed to M.D.K.